AFRL-AFOSR-JP-TR-2016-0066

Comparison between hydrogen and methane fuels in a 3-D scramjet at Mach 8

Michael Kevin Smart
THE UNIVERSITY OF QUEENSLAND

06/24/2016
Final Report

Air Force Research Laboratory
AF Office Of Scientific Research (AFOSR)/ IOA
Arlington, Virginia 22203
Air Force Materiel Command

REPORT DOCUMENTATION PAGE

Form Approved
OMB No. 0704-0188

1. REPORT DATE *(DD-MM-YYYY)*	2. REPORT TYPE	3. DATES COVERED *(From - To)*
24-06-2016	Final	01 Apr 2013 to 27 Mar 2015

4. TITLE AND SUBTITLE
Comparison between hydrogen and methane fuels in a 3-D scramjet at Mach 8

5a. CONTRACT NUMBER

5b. GRANT NUMBER
FA2386-13-1-4060

5c. PROGRAM ELEMENT NUMBER
61102F

6. AUTHOR(S)
Michael Kevin Smart

5d. PROJECT NUMBER

5e. TASK NUMBER

5f. WORK UNIT NUMBER

7. PERFORMING ORGANIZATION NAME(S) AND ADDRESS(ES)
THE UNIVERSITY OF QUEENSLAND
UNIVERSITY OF QUEENSLAND
BRISBANE, 4072 AU

8. PERFORMING ORGANIZATION REPORT NUMBER

9. SPONSORING/MONITORING AGENCY NAME(S) AND ADDRESS(ES)
AOARD
UNIT 45002
APO AP 96338-5002

10. SPONSOR/MONITOR'S ACRONYM(S)
AFRL/AFOSR IOA

11. SPONSOR/MONITOR'S REPORT NUMBER(S)
AFRL-AFOSR-JP-TR-2016-0066

12. DISTRIBUTION/AVAILABILITY STATEMENT
A DISTRIBUTION UNLIMITED: PB Public Release

13. SUPPLEMENTARY NOTES

14. ABSTRACT
Gaseous hydrogen has typically been the fuel of choice for scramjets operating at speeds greater than Mach 7. This is because of its high specific energy content, as well as its fast reaction characteristics in air. The disadvantage of hydrogen is its low density, which is a particular problem for small vehicles with significant internal volume constraints. The current study investigated the use of gaseous methane as a fuel for a Mach 8 scramjet. This involved experiments with a 3-D scramjet using a cavity based flame holder in the T4 shock tunnel at The University of Queensland, as well as a companion fundamental CFD study. The performance of small chained hydrocarbons (ethylene and methane) was compared with hydrogen to establish the importance of its lower specific energy content and slower reaction characteristics. In addition, a scoping study was performed to determine the capability for direct connect testing in the T4 shock tunnel.

15. SUBJECT TERMS
Airbreathing Engines, Hypersonics, Propulsion, AOARD

16. SECURITY CLASSIFICATION OF:			17. LIMITATION OF ABSTRACT	18. NUMBER OF PAGES	19a. NAME OF RESPONSIBLE PERSON
a. REPORT	b. ABSTRACT	c. THIS PAGE			KNOPP, JEREMY
Unclassified	Unclassified	Unclassified	SAR	50	19b. TELEPHONE NUMBER *(Include area code)* 315-227-7021

Standard Form 298 (Rev. 8/98)
Prescribed by ANSI Std. Z39.18

YEAR 2 Progress Report

Comparison between hydrogen, methane and ethylene fuels in a 3-D Scramjet at Mach 8

Professor Michael K. Smart
Chair of Hypersonic Propulsion
The University of Queensland
m.smart@uq.edu.au

Dr. Vincent Wheatley
Senior Lecturer
The University of Queensland
v.wheatley@uq.edu.au

Dr. Anand Veeraragavan
Lecturer
The University of Queensland
anandv@uq.edu.au

Executive Summary

Gaseous hydrogen has typically been the fuel of choice for scramjets operating at speeds greater than Mach 7. This is because of its high specific energy content, as well as its fast reaction characteristics in air. The disadvantage of hydrogen is its low density, which is a particular problem for small vehicles with significant internal volume constraints. The current study investigated the use of gaseous methane as a fuel for a Mach 8 scramjet. This involved experiments with a 3-D scramjet using a cavity based flame holder in the T4 shock tunnel at UQ, as well as a companion fundamental CFD study. The performance of small chained hydrocarbons (ethylene and methane) was compared with hydrogen to establish the importance of its lower specific energy content and slower reaction characteristics. In addition, a scoping study was performed to determine the capability for direct connect testing in the T4 shock tunnel.

Project Status

The project has successfully delivered on its objective of experimentally demonstrating repeatable ignition of a low order hydrocarbon fuel in a realistic 3D scramjet engine at Mach 8. This has been made possible by the high quality team that has been involved. As well as Professor Smart and Dr Wheatley, the participants are:

- Dr Anand Veeraragavan – Combustion
- Dr Stefan Brieschenk – spark ignition system
- Mr Zachary Denman – PhD student

The Milestones for the project are listed in Appendix 1. The status of the milestones is as follows:

Experimental

The cavity designed in year 1 was tested in UQ's T4 tunnel late last year. Three fuels (hydrogen, methane and ethylene) were tested. Successful ignition was demonstrated for hydrogen and ethylene.

Computational

Axisymmetric pre-mixed computations were improved since year 1 to include a diverging combustor. Fuel mixing studies have been initiated to better understand the operation with the cavity combustor.

Direct Connect Facility Scoping Study

A configuration for operating T4 as a direct-connect facility has been established. A report on this, including budgetary numbers, is on schedule for completion in July 2014. This study is included here as Appendix 2.

Outputs

Two conference papers on the research supported by this grant were presented at the AIAA Hypersonics and Spaceplanes conference held in Atlanta in June 2014.

One journal paper on the results from the successful test campaign is in the final stages of preparation to be submitted to the AIAA Journal of Propulsion and Power. The PhD student whose research delivered on the objectives of this grant, is on track to progress on internal milestones towards completion.

1. Introduction

Scramjets are air-breathing engines where combustion occurs at supersonic speeds. Since the flow remains supersonic, the residence time of the flow within scramjet engines operating beyond Mach 7 is usually on the order of a millisecond. In this time, fuel injection, mixing, ignition, and combustion must occur. To be able to burn unaided under these conditions, a fuel with short ignition delay time is required, while a fuel with high energy per unit-mass is desirable to maximize specific impulse [1]. These desired characteristics have led to gaseous hydrogen typically being the fuel of choice for scramjets operating at speeds greater than Mach 7. The low energy per unit volume of gaseous hydrogen, however, is a significant problem for small vehicles with internal volume constraints, in addition to the difficulties associated with its storage and handling. This necessitates research into other fuels in the supersonic combustion regime. Low-order hydrocarbon fuels, such as ethylene and methane, both have much greater energy per unit volume as well as the advantage of easier handling and storage [1]. Table 1 highlights the differences in the energy densities per unit mass and per unit volume for the low-order hydrocarbons considered, as well as hydrogen.

Table 1: Energy properties of low-order hydrocarbons and hydrogen [1, 2]

Fuel	Energy/Mass (MJ/kg)	Energy/Volume (MJ/L)	STP Density (kg/m^3)
Hydrogen	116.7	8.2	71
Methane	50.0	20.8	424
Ethylene	47.2	26.8	568

This is better represented on a normalised basis in Figure 1. It is clear that lower order hydrocarbons possess highly favourable density and energy density, which can extend the range for volume-constrained, frame integrated scramjets.

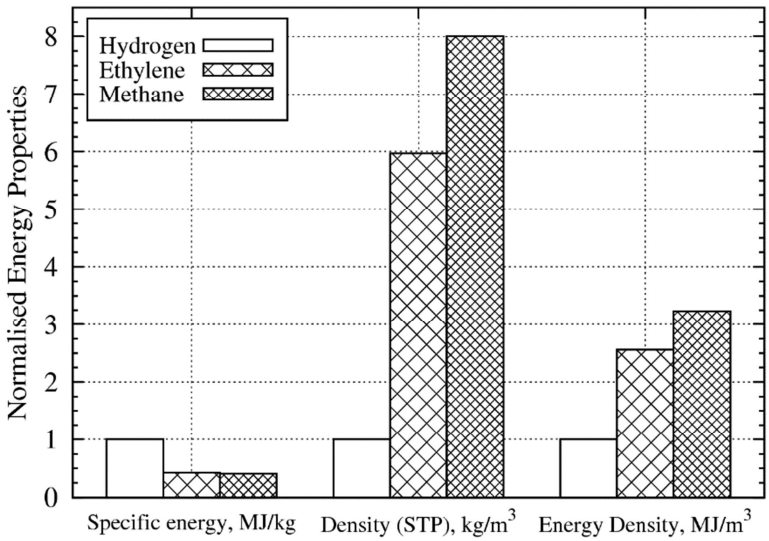

Figure 1: Normalised comparison of physical and energetic properties of hydrogen, methane and ethylene.

While their energy per unit volume and handling requirements are favourable, low-order hydrocarbons have much greater ignition delay times than hydrogen [3]. Due to this, the use of

hydrocarbon fuels would require much longer non-recirculating, spontaneous ignition combustors to complete combustion.

The current study investigated the use of gaseous methane and ethylene as a fuel for a Mach 8 scramjet. This was conducted via shock tunnel experiments with a 3-D scramjet. The inlet geometry of the scramjet is based on the Rectangular-to-Elliptical Shape Transition (REST) configuration of Smart [4]. This fixed geometry, mixed-compression configuration, transitions smoothly from a quasi-rectangular capture shape to an elliptical throat. In combination with a divergent elliptical combustion chamber, REST inlets have been shown to produce a useful flowpath for hypersonic applications [5]. The current configuration is an exploratory Mach 8.1 point design flowpath which has been explicitly adapted for fuel injection in the inlet. This engine has been previously tested with gaseous hydrogen as the fuel [6]. The proposed experiments will involve the addition of a cavity based flame holder and a spark ignition system to the flowpath, and testing with gaseous hydrogen, ethylene and methane.

2 Cavity combustor design

Figure 2 shows the schematic of a cavity flameholder in which the geometric parameters depth (D), length (L) and aft-wall angle (θ) are variables that must be carefully chosen based on physical reasoning/models in order to be able to ignite and hold the flame for a certain fuel type.

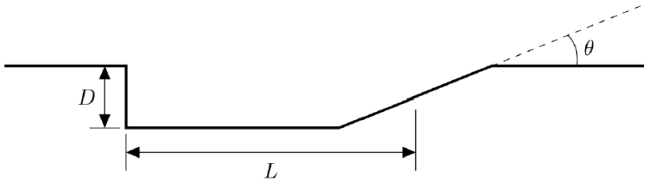

Figure 2: Schematic of cavity flameholder

Previous testing of a cavity with a L/D ratio of 4.0 and an aft-wall angle (θ) of 22.5 degrees was performed at the AFRL. These cavity dimensions lie within the open cavity regime, as well as the range for a cavity with a stable flowfield and minimum drag. As the depth of the cavity is proportional to the residence time of the cavity, Davis and Bowersox's relation for cavity depth (Equation 1) coupled with Colket and Spadaccini's ignition delay time correlation (Equation 2), may be used to estimate the required depth of the cavity.

$$D = \frac{\tau_r U_\infty}{40} \tag{1}$$

$$\tau_{ign} = A \exp\left(\frac{E}{R_u T}\right) [O_2]^a [C_x H_y]^b \tag{2}$$

As the ignition delay time of a combustible mixture is highly dependent on temperature, the temperature within the cavity must first be estimated. This was done using axisymmetric RANS simulations in the University of Queensland's hypersonic flow solver, Eilmer3 . A nominal cavity depth of 4.4 mm was simulated; this cavity has an identical depth to combustor hydraulic diameter ratio as a previously tested cavity . The simulations used the $k-\omega$ turbulence model and assumed a

thermally perfect gas. In the simulations, the combustor is initially filled with low pressure quiescent air with a temperature of 300 K and a pressure of 66.5 Pa to match the conditions in the test section of the facility prior to the arrival of the test flow. A supersonic inflow boundary condition on the inlet of the domain supplies the flow state expected at the Mach 8 REST combustor entrance (flow conditions shown in Table 2. The pressure difference between the inflow boundary and the initial fill gas drives a strong shock wave through the combustor, mimicking the shock tunnel start-up process. The inflow turbulence intensity and laminar-to-turbulent viscosity ratios were 0.01 and 1.0, respectively. The turbulent Prandtl and Schmidt numbers were set to 0.89 and 0.75, respectively. The grid was refined to a point where the centers of the cells adjacent to walls had y^+ less than one. A fixed temperature boundary condition ($T_{wall} = 300$ K) was used along all combustor surfaces, corresponding to testing in an impulse facility, and an extrapolation boundary condition was applied at the outflow.

Table 2: Flow conditions for CFD.

Temperature (K)	Pressure (kPa)	Velocity (m/s)
932	47.9	2005

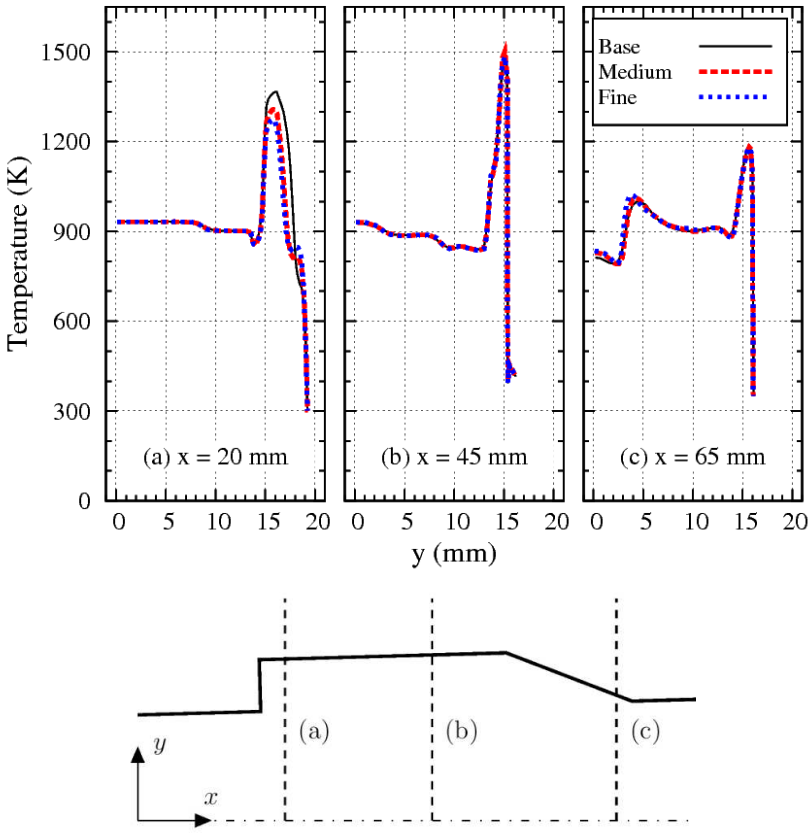

Figure 3: Temperature profile at different axial locations throughout axisymmetric cavity flameholder.

Simulations were run on a 29,200 cell base grid. To evaluate the adequacy of this resolution, the reference simulation was repeated with grid refinement ratios of $3/2$ and 2. The convergence of the average outflow static temperature and streamwise momentum flux were examined using

generalised Richardson extrapolation for unequal refinement ratios. The order of convergence of these statistics was two in both cases, with the convergence being monotonic. For the simulation on the fine grid, the average static temperature and momentum flux differ from their Richardson extrapolated values by -0.2% and 1.9%, respectively. This demonstrates that the effect of discretisation error on the solution is acceptably small. Figure 3 shows the temperature profile at various points within the cavity. The profiles for the base, medium, and fine grids are shown at three locations. There is very good agreement between the medium and fine grids at all locations. This indicates that the domain is sufficiently resolved by the medium grid. Simulations were run for 0.5 ms of flow time. At this point, the maximum volume-weighted ℓ^2 norm of temperature and pressure across the domain vary by 0.02% and 0.08% of the freestream properties, for the medium grid.

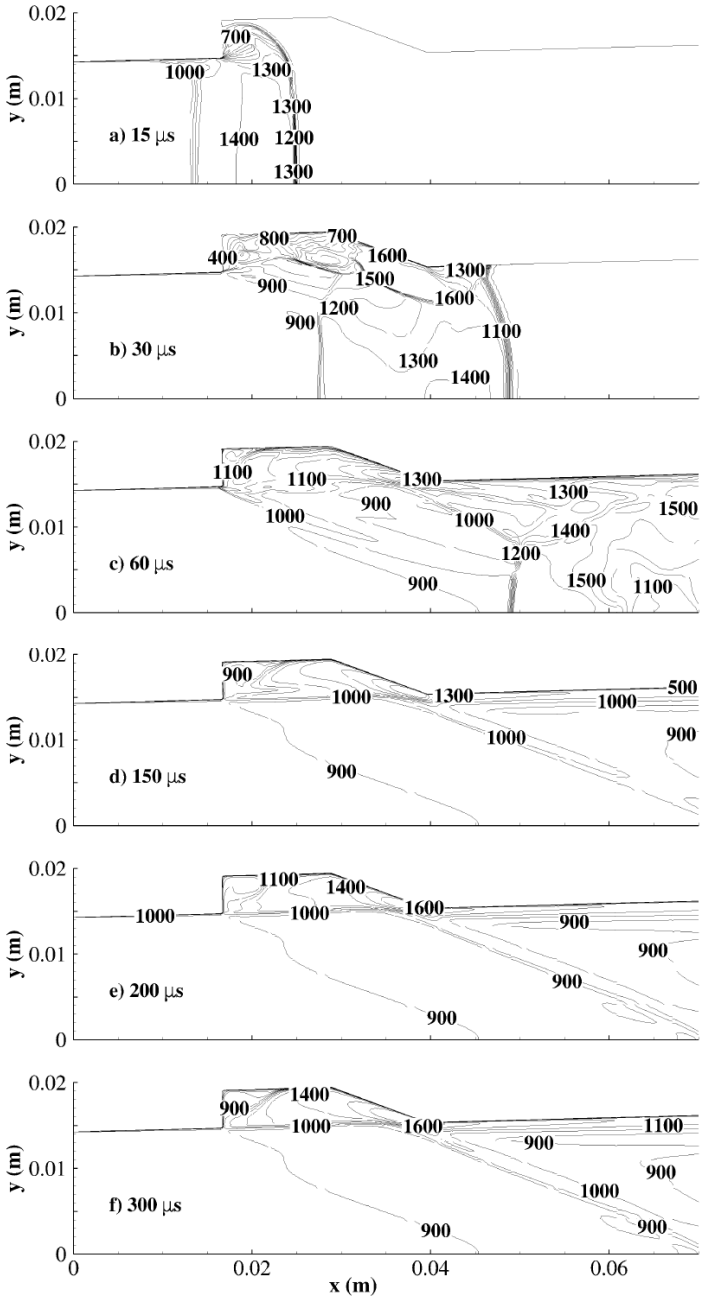

Figure 4 Temperature contours in an axisymmetric, unfueled, simulation of cavity flameholder in diverging combustor at various times.

Figure 4 shows the temperature contours of the flow within the cavity at various times throughout the simulation; the full domain is 200 mm long. The temperature and pressure (mass-weighted) in the "core" of the cavity are 1490 K and 37.1 kPa, respectively. The "core" temperature of the cavity was determined by excluding temperatures in the thermal boundary layer that were below the average temperature ($T_{avg} = 1290$ K) of the flow within the cavity. Comparison of Fig. 4d and Fig. 4e shows that the cavity flowfield is well established by 150 μs. Over the next 150 μs (Fig. 4f), the flow behind the rearward facing step is further heated, but the overall flowfield within the cavity is relatively unchanged. The core temperature within the cavity was used to estimate the ignition delay time for ethylene, methane, and hydrogen in the engine.

Figure 5 shows the residence time of a cavity as a function of cavity depth using Eq. 1 and Eq. 2 Davis and Bowersox's relation divides the domain into two regions; flameholding and non-flameholding. The ignition delay times of hydrogen and ethylene (at the cavity core temperature and pressure) are shown as horizontal lines; the ignition delay time of methane is approximately 2 ms at the core temperature and pressure, which is too long for the experimental model and suggests forced ignition is necessary for methane. The intersection of these lines and Davis and Bowersox's relation, indicates the minimum depth required for an auto-igniting cavity for that fuel, at the conditions noted. The minimum depth required for a cavity that will auto-ignite ethylene, based on the temperature and pressure in the cavity from the axisymmetric simulations, is approximately 4 mm. Using this design methodology, a cavity depth of 100 mm is required for methane, at the core temperature and pressure, which is far too large to be incorporated into the engine geometry.

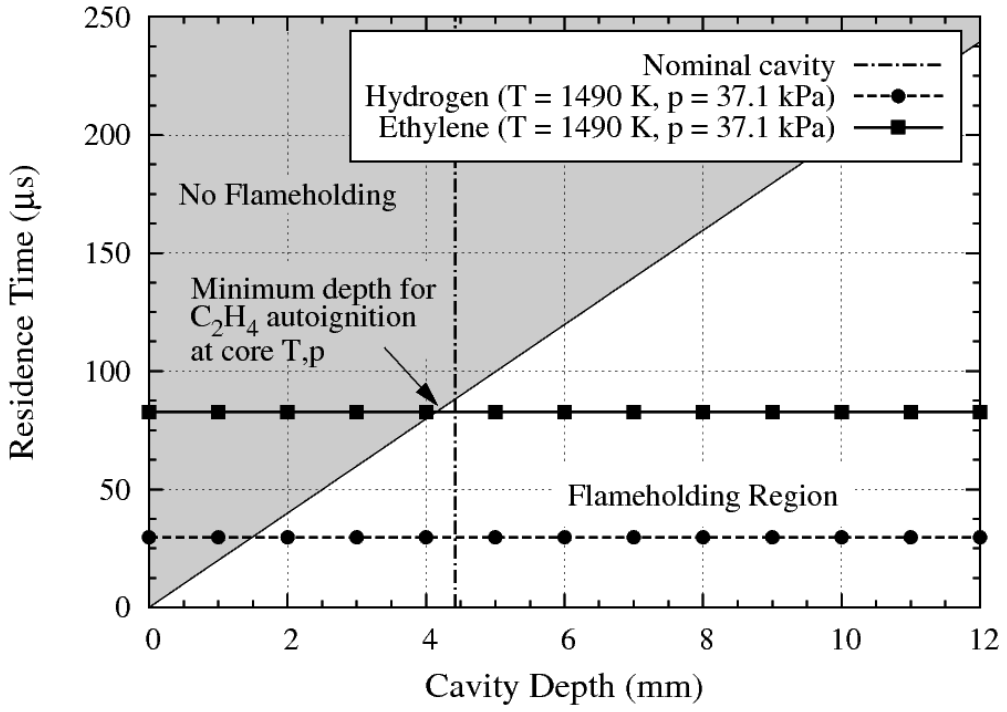

Figure 5: Depth of cavity based on Davis and Bowersox relation, coupled with Colket and Spadaccini's ignition delay correlations for hydrogen and ethylene with $\phi = 0.7$.

4. Experiments

4.1 Experimental Model

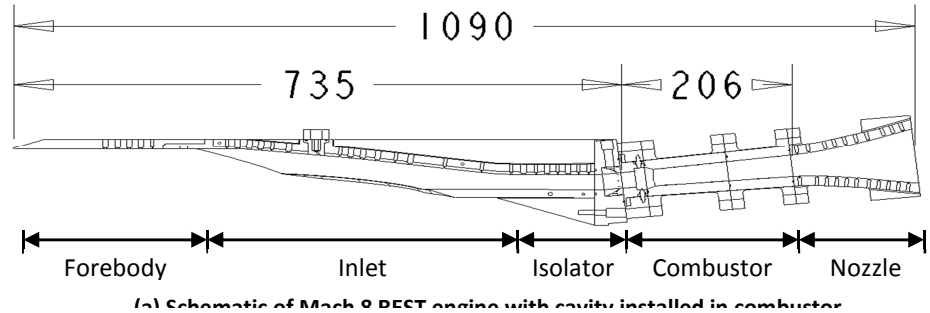

(a) Schematic of Mach 8 REST engine with cavity installed in combustor

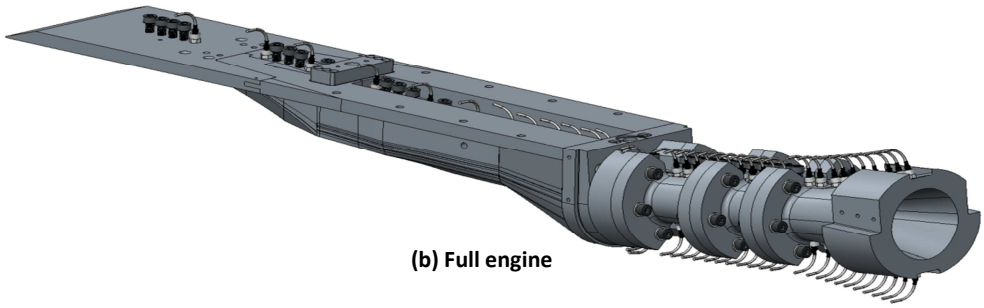

(b) Full engine

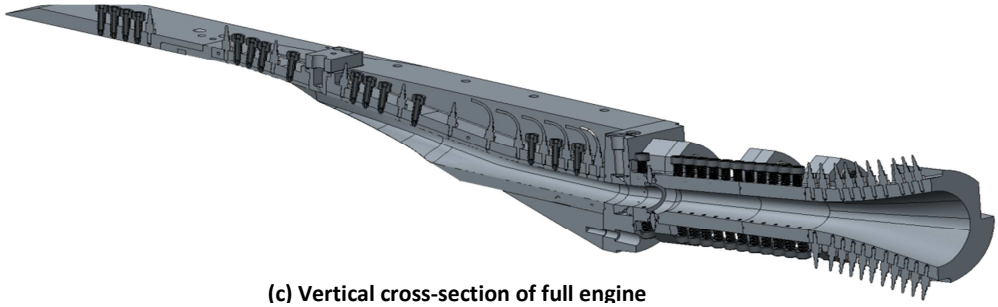

(c) Vertical cross-section of full engine

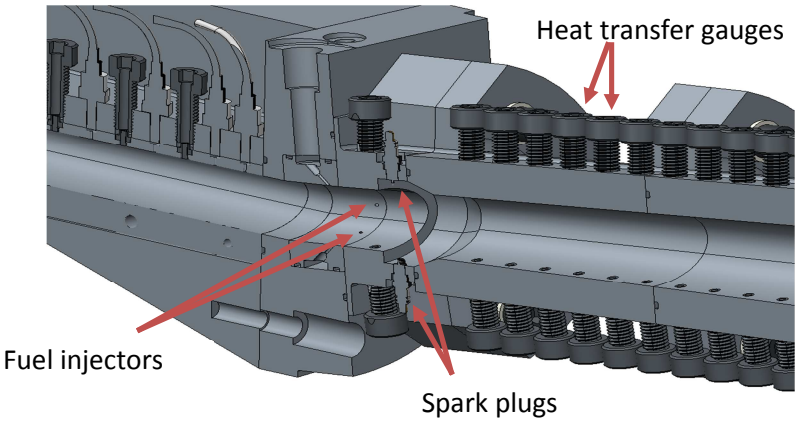

(d) Zoomed view of vertical cross-section showing cavity (pressure transducers are on opposite side of vertical plane)

Figure 5: Schematic and computer-aided design images of modified Mach 8

A schematic of the scramjet engine tested is provided in Figure 5. The experimental model is approximately 1100 mm long and 150 mm wide. The model has four main components; a steel forebody, a Mach 8 REST inlet, a combustor with cavity flameholder, and nozzle. During testing the model is inclined at 6° to the incoming flow to allow for freejet testing. The REST inlet has an overall

geometric contraction ratio of 5.80 and an internal contraction ratio of 1.99. A constant-area section, 110 mm long is included as part of the inlet. The combustor and nozzle are 229 mm and 150 mm in length, and diverge uniformly with area ratios of 2.0 and 2.5, respectively.

Fuel can be injected on the inlet through three equally spaced 1.613 mm diameter porthole injectors or at the combustor entrance through eight equally spaced 1.041 mm diameter porthole injectors. All injectors are inclined at 45° to the local flow direction. All results presented are for the combustor-only fueled experiments.

4.2 Experimental Campaign

The experiments that form part of this investigation were conducted in the T4 Reflected Shock Tunnel at the University of Queensland in Brisbane. The T4 Facility is a large reflected shock tunnel facility which utilises a 92 kg piston and is capable of producing flows with stagnation enthalpies from 2.5-15 MJ/kg with nozzle supply pressures ranging from 10-90 MPa [20]. A schematic of the facility is shown in Figure 6.

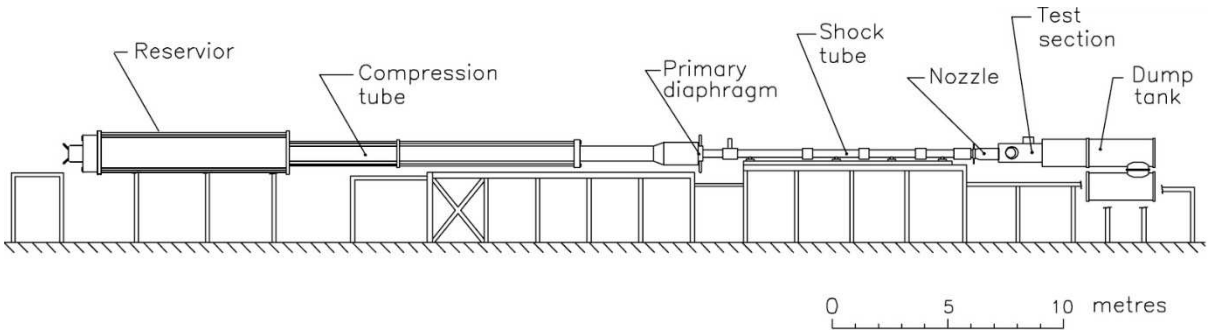

Figure 6: Schematic of the T4 Reflected Shock Tunnel at the University of Queensland

The experimental campaign will be used to determine the effect the cavity has on the performance of the engine. Both ethylene and methane will be tested, with and without spark ignition. The results of these tests will be compared to previous experimental campaigns with the original Mach 8 REST engine (no cavity in the combustor), to determine the effect the cavity and spark ignition have on combustion. The test flow conditions and flow properties are shown in Table 3.

Table 3 Nominal experimental and flight conditions

Nozzle-supply conditions			Derived freestream conditions					Flight conditions		
p_s	T_s	H_s	p_e	T_e	u_e	M_e	γ_e	M_f	h_f	q_f
MPa	K	MJ/kg	kPa	K	m/s	–	–	–	km	kPa
20.8	2500	2.65	1900	231	2330	7.64	1.40	7.32	28.7	53.5

Figure 7 shows the scramjet engine model mounted in the T4 shock tunnel prior to testing. The side view photograph (Fig. 7a) shows the engine mounted to the underside of the instrumentation box (bluish-green box), while front view photograph (Fig. 7b) shows the rectangular intake of the REST engine.

(a) Side view

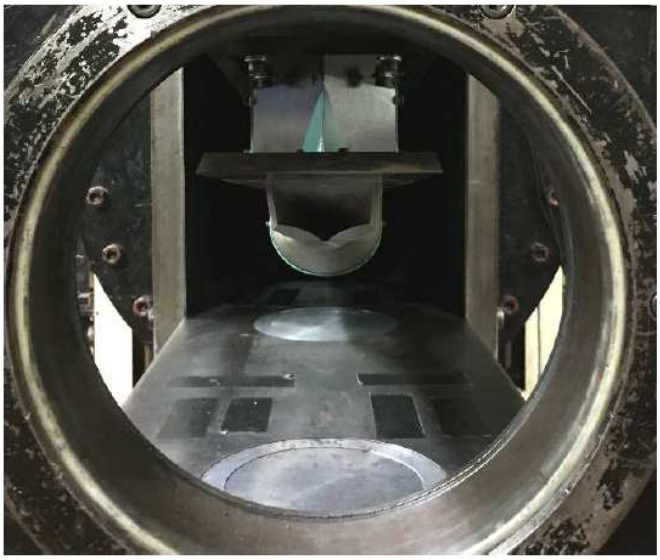

(b) Front view

Figure 7: Experimental model in the test section.

Results and Discussions

The following section will outline the results of the experiments. The discussions in this section will be limited to the combustor-only fueled experiments. Firstly, the inclusion of a cavity flameholder will be examined, followed by fuel-off and suppressed-combustion experiments. After this, the ethylene-fueled experiments will be discussed. Finally, the performance of hydrogen, ethylene, and methane fuels will be compared.

In the plots of pressure distribution in the following sections, a schematic of the engine is shown above all plots with the combustor injection location ($x = 725$ mm) shown by a vertical dashed line. All pressure measurements have been normalized by the freestream pressure (viz. facility nozzle-exit pressure), p_e corresponding to each test.

Fuel-off experiments with and without cavity flameholder

Previous testing with this engine, without a cavity flameholder has been performed. With the inclusion of a cavity flameholder at the beginning of the combustor, it is important to establish a new baseline measurement for the pressure within the flowpath. Figure 8 shows results from

previous testing without a cavity flameholder (shot 11413) and the current testing with a cavity (shot 11692).

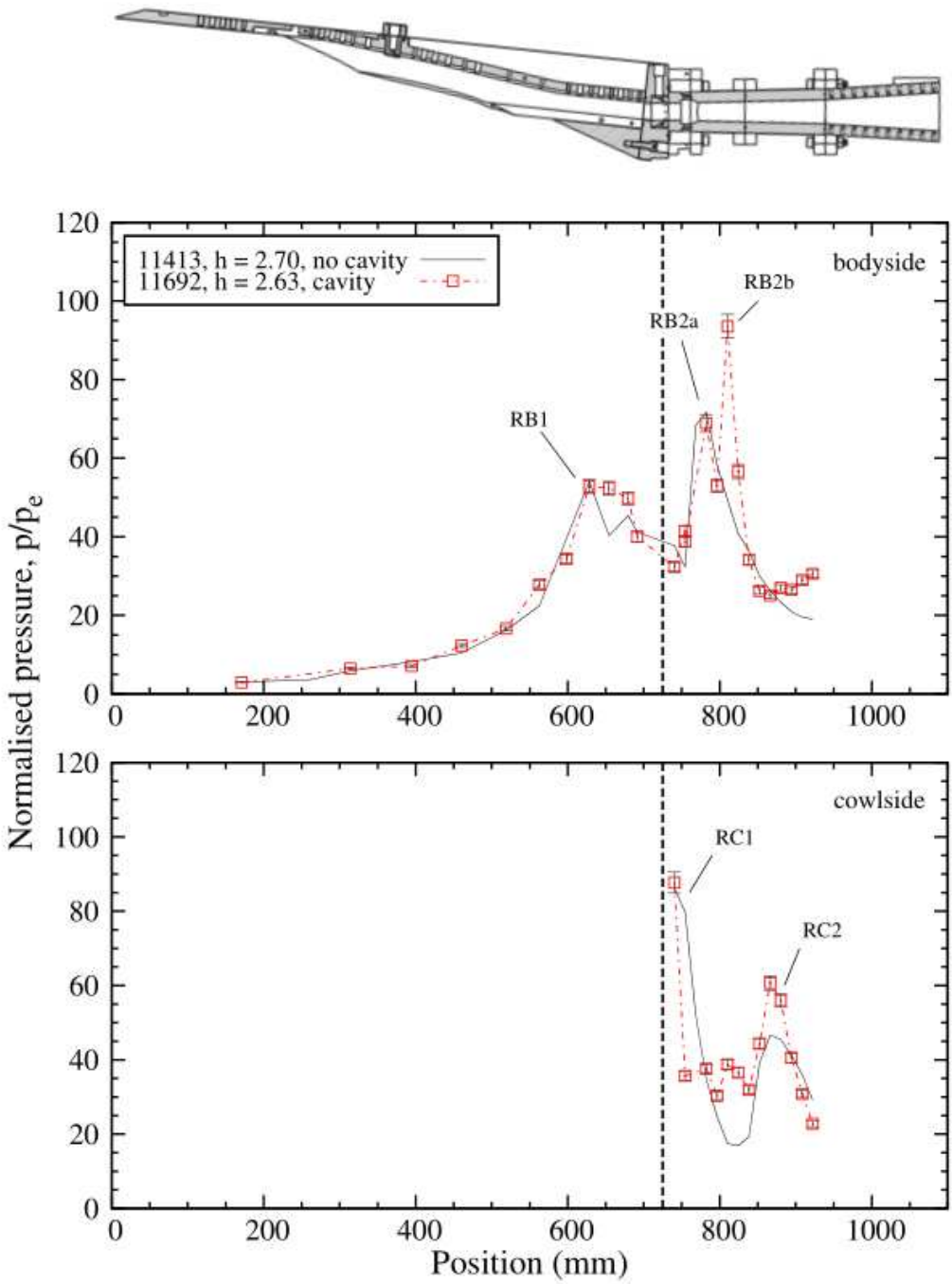

Figure 8: Fuel-off comparison, with and without cavity flameholder

The pressure distributions for both shots in Fig. 8 along the bodyside of the inlet match very closely. These experiments were performed nearly fifteen months apart and the agreement shown in these traces provides a good indication that the integration of the experimental model into facility has been performed in a consistent manner. The distributions have been truncated at the combustor exit due to the two experiments having used different nozzles. The most noticeable difference between the two pressure distributions is the large secondary peak (RB2b) that occurs on the

bodyside of the engine at $x = 810$ mm with the introduction of the cavity flameholder. As the smaller upstream peak, at $x = 782$ mm, is present in both experiments in Fig. [fig:cavity-vs-no-cavity], it is most likely the second reflection shock of the cowl shock on the bodyside of the engine, indicated by RB2a. This new, larger peak (RB2b), can therefore, be associated with the inclusion of the cavity flameholder in the combustor. The cavity flameholder generates a strong recompression shock from its aft-wall; this spike in pressure is, very likely, caused by this shock. Downstream of this shock, the pressure recovers to approximately the same level as in the experiment with no cavity. Changes to the pressure distributions are also evident on the cowl side of the engine. The large spike in pressure (RC1) is still present just downstream of the injection location. The drop from this high level occurs earlier compared to previous tests without the cavity

Ethylene-fueled experiments

The results of the ethylene-fueled experiments are shown in Figure 9. Ignition and combustion of ethylene was achieved for all equivalence ratios tested. Pressure distributions from three fuel-on experiments at varying equivalence ratio are shown (shots 11697, 11698 and 11700) with an experiment where combustion was suppressed (shot 11701) by using a nitrogen test gas, instead of air. The pressure distributions in Fig. 9 clearly show an increase from a combustion-induced pressure rise from $x = 850$ mm to the nozzle exit, when compared to the combustion-suppressed shot. This increase is evident in both the bodyside and cowlside pressure distributions. The pressure rise occurs approximately 90 mm downstream of the cavity. It is possible that the flow is ignited by the recompression shock downstream of the cavity.

A marginally higher pressure is seen at a majority of sensor locations in the pressure distribution corresponding to a higher equivalence ratio (shot 11698). Peak pressures on the bodyside are relatively unaffected by equivalence ratio, but the pressure rise is maintained further downstream. The spikes in the pressure distribution on the cowlside of the engine indicate the flowfield to be shock-dominated. However, both sides of the engine show the aforementioned pressure rise for the fuel-into-air shots over the combustion-suppressed shots.

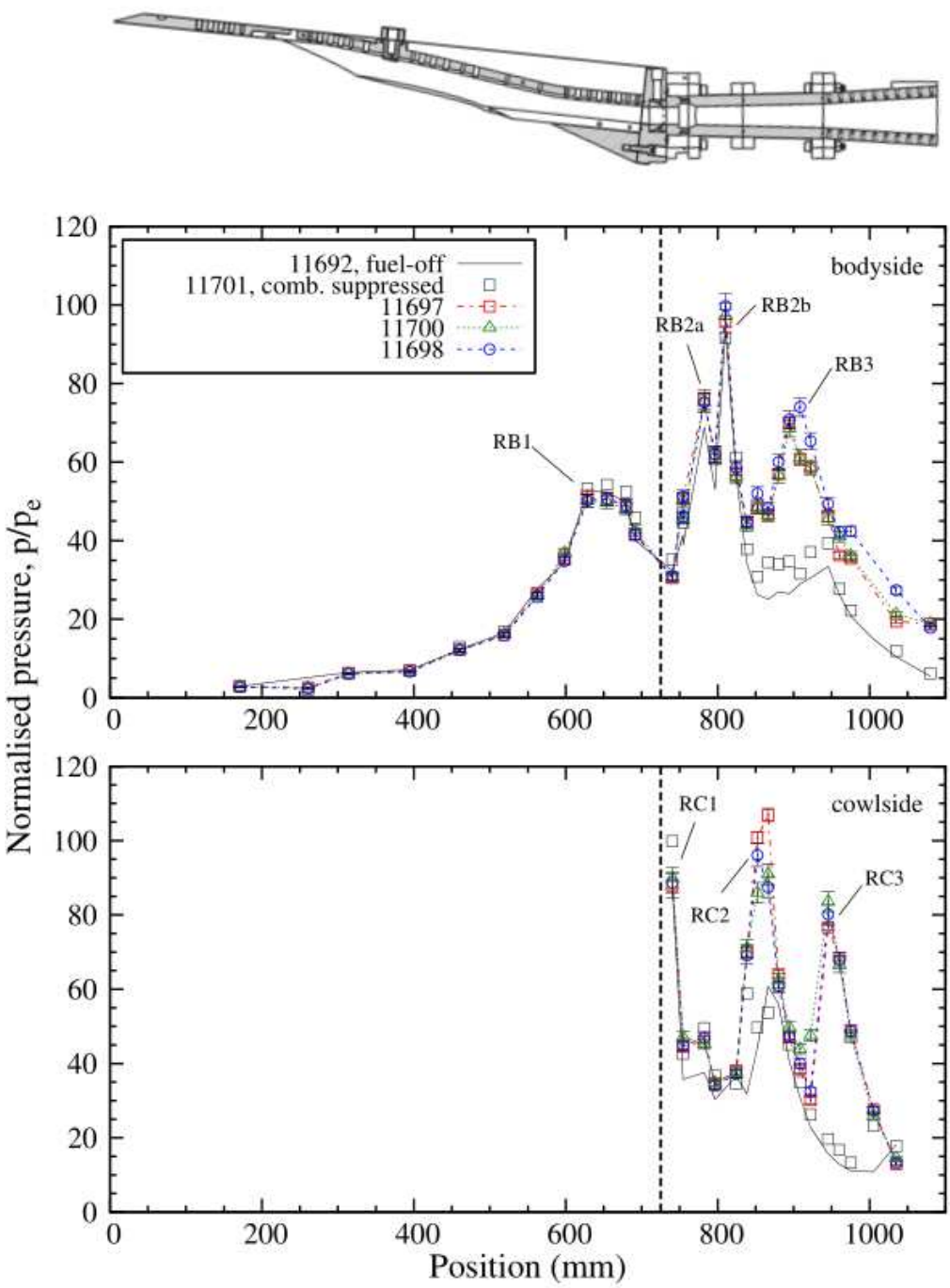

Figure 9: Ethylene-fueled experiments.

Methane-fueled experiments

When methane is injected, there is no observable combustion-induced pressure rise; only pressure rise due to mass addition is evident. This can be seen by comparison of shots 11713, 11714, and 11715 of Figure 10, the last of which, has had combustion suppressed through the use of a nitrogen test gas. Due to the methodology used to design the cavity flameholder, methane was not expected to auto-ignite. Methane fueled experiments were still conducted, however, to verify the need for forced ignition for this fuel choice.

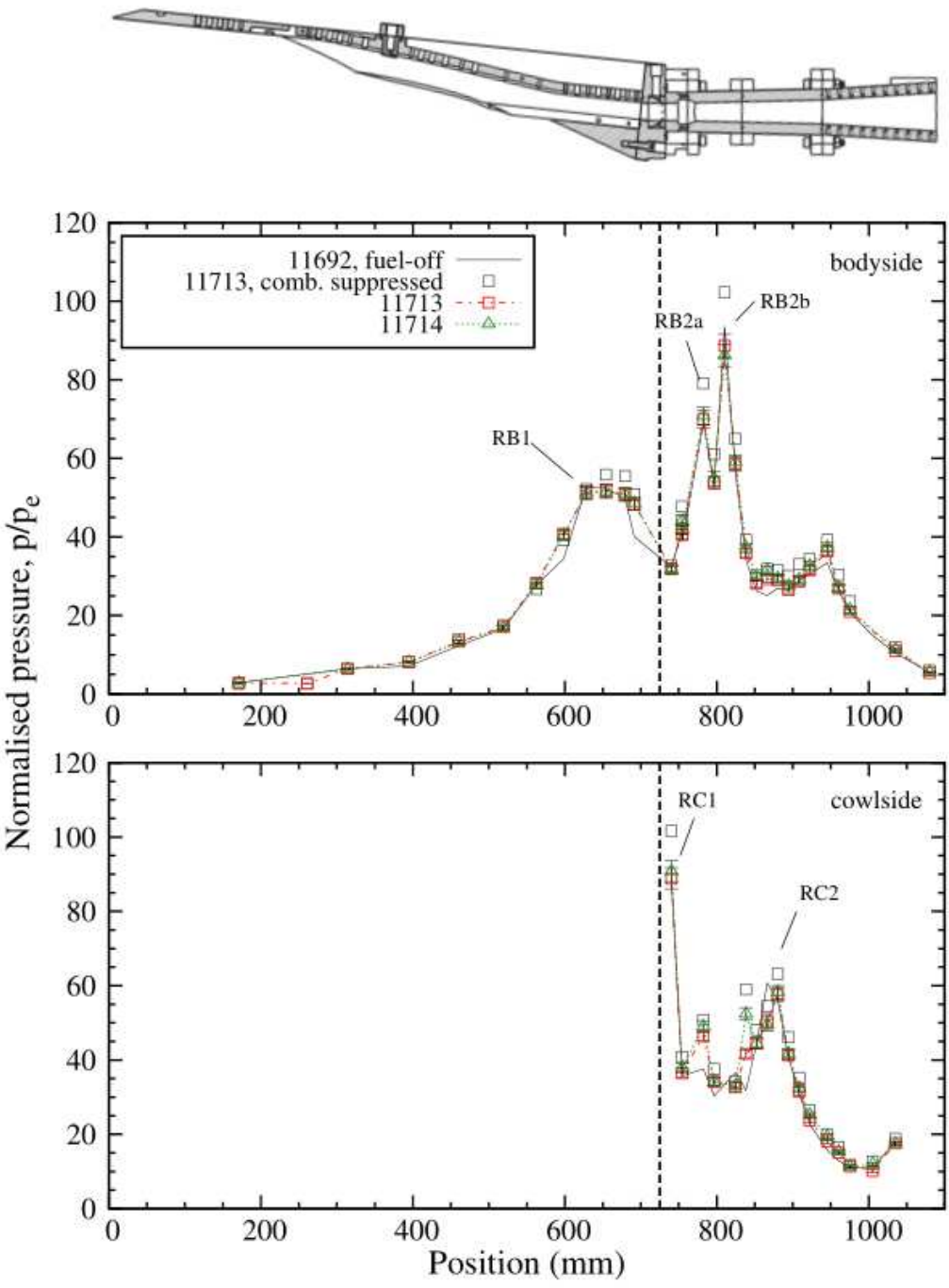

Figure 10: Methane-fueled experiments

Comparison of fuels

The pressure distributions for hydrogen (shot 11727), ethylene (shot 11700), and methane (shot 11714) are shown in Figure 11. The pressure distributions upstream of the injection point ($x = 725$ mm) are near identical, as expected. The pressure distributions vary greatly following the injection of fuel at the combustor entrance. A fuel-off shot is used for comparison (shot 11692), as the three fuels only exhibit small differences between their associated suppressed-combustion shots.

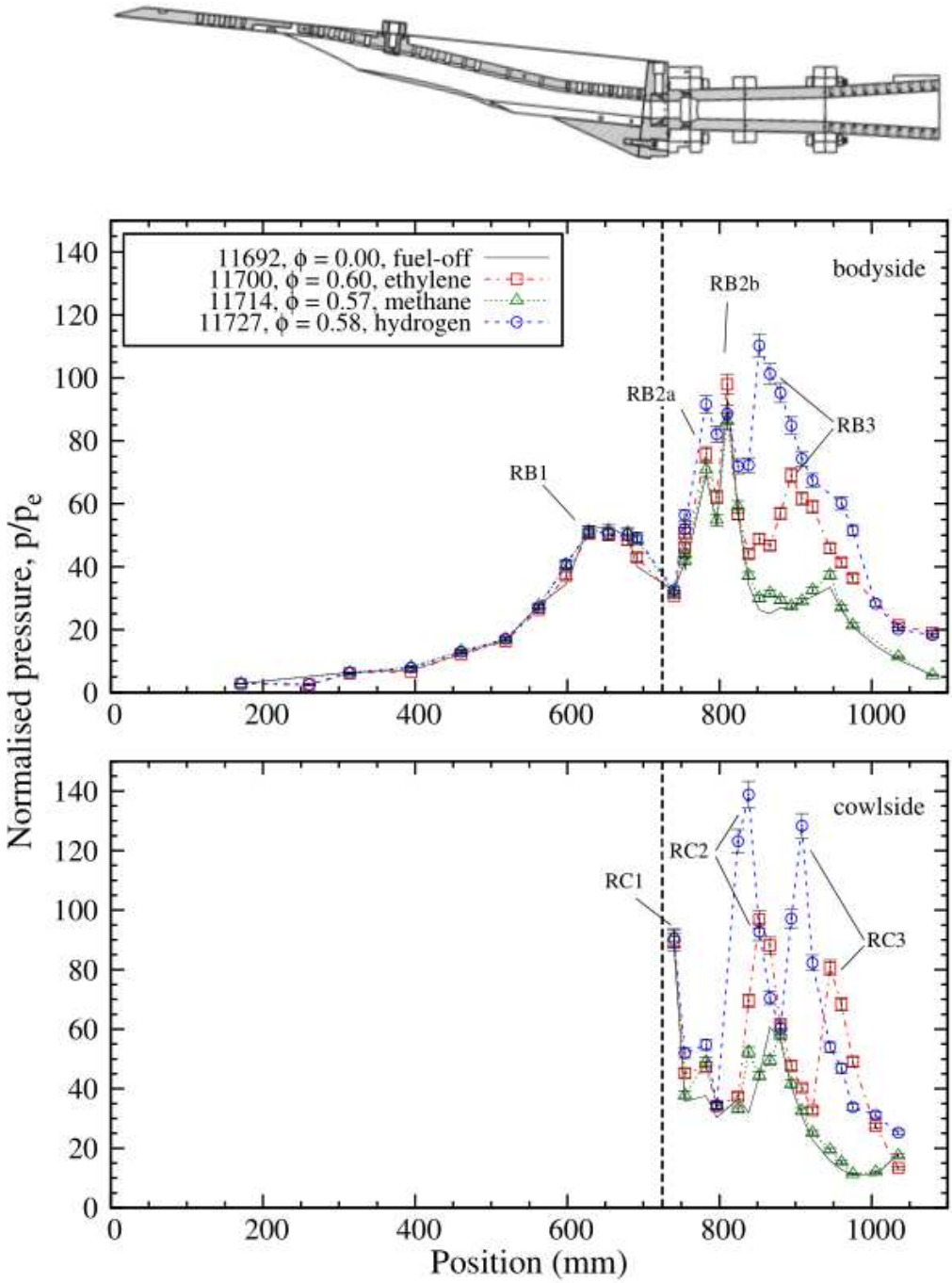

Figure 11: Comparison of fuels tested

As discussed in the ethylene fuelled experiments section, ethylene ignites and burns from $x = 850$ mm on both the body and cowlside of the engine, with the flowfield on the cowlside of the engine being heavily shock-dominated. The pressure distribution from the hydrogen-fueled experiment shown in Fig. 11 shows hydrogen igniting at the cavity flameholder ($x = 750$ mm). The ignition of hydrogen also occurs approximately 25 mm earlier than ethylene, which occurs at 800 mm and 825 mm, respectively. The flowfield downstream of the cavity appears to have been altered by the combustion of hydrogen at the cavity. The recompression shock of the cavity (RB2b) appears to

arrest the combustion of hydrogen immediately downstream of the cavity; the normalized pressure drops to combustion-suppressed levels.

Both hydrogen and ethylene achieve the same pressure rise on the body side of the engine from 1000 mm to the end of the flowpath. This could suggest that although ethylene ignites further downstream then hydrogen, it may burn just as completely as hydrogen. On the cowlside of the engine, ethylene exhibits a higher pressure for the most of the nozzle, however, the pressure drops to suppressed combustion levels by the nozzle exit.

Spark Ignition Testing

Since the methane fuelled cases failed to ignite, we next investigated testing this fuel with a spark ignition system. The results from these are shown in Figures 12 and 13 for methane-air and ethylene-air shots respectively. The combined spark ignition energy was around 300 mJ in total at a frequency of 61 Hz such that there was one "spark event" during the test time.

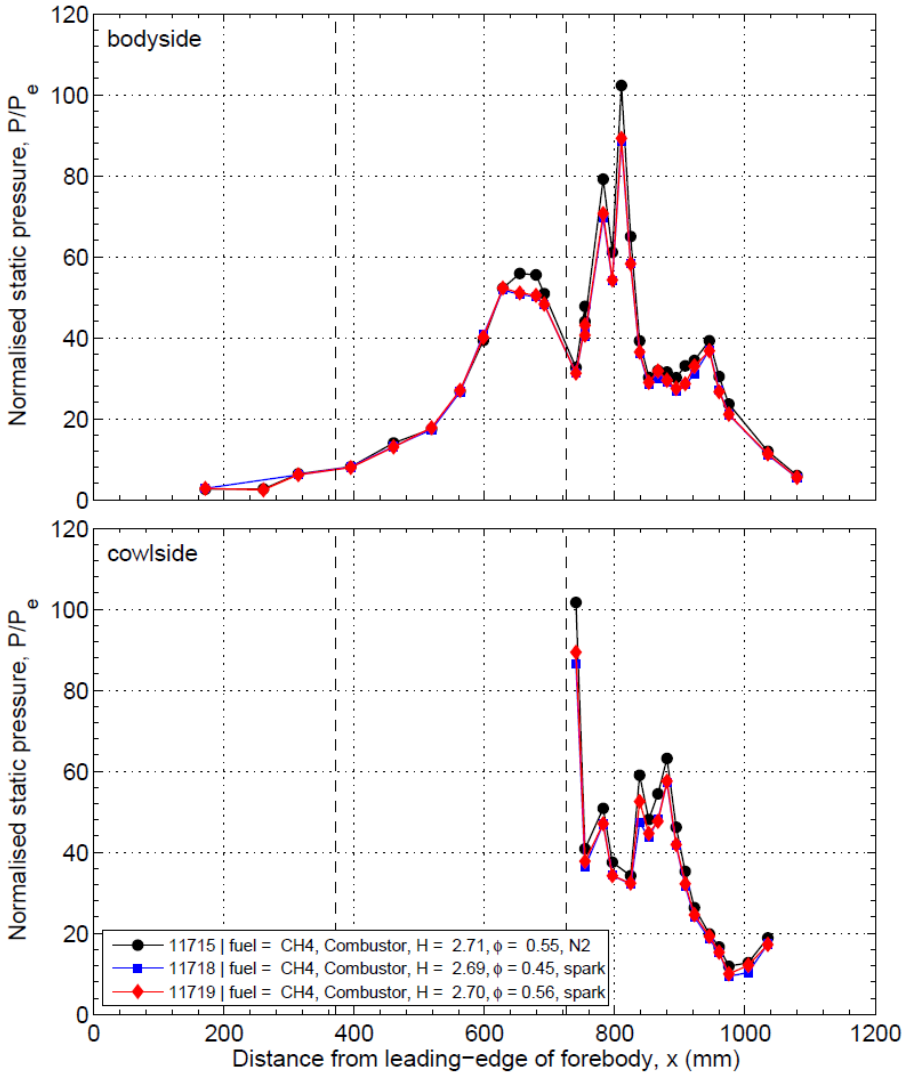

Figure 12: Spark ignition testing of methane-air

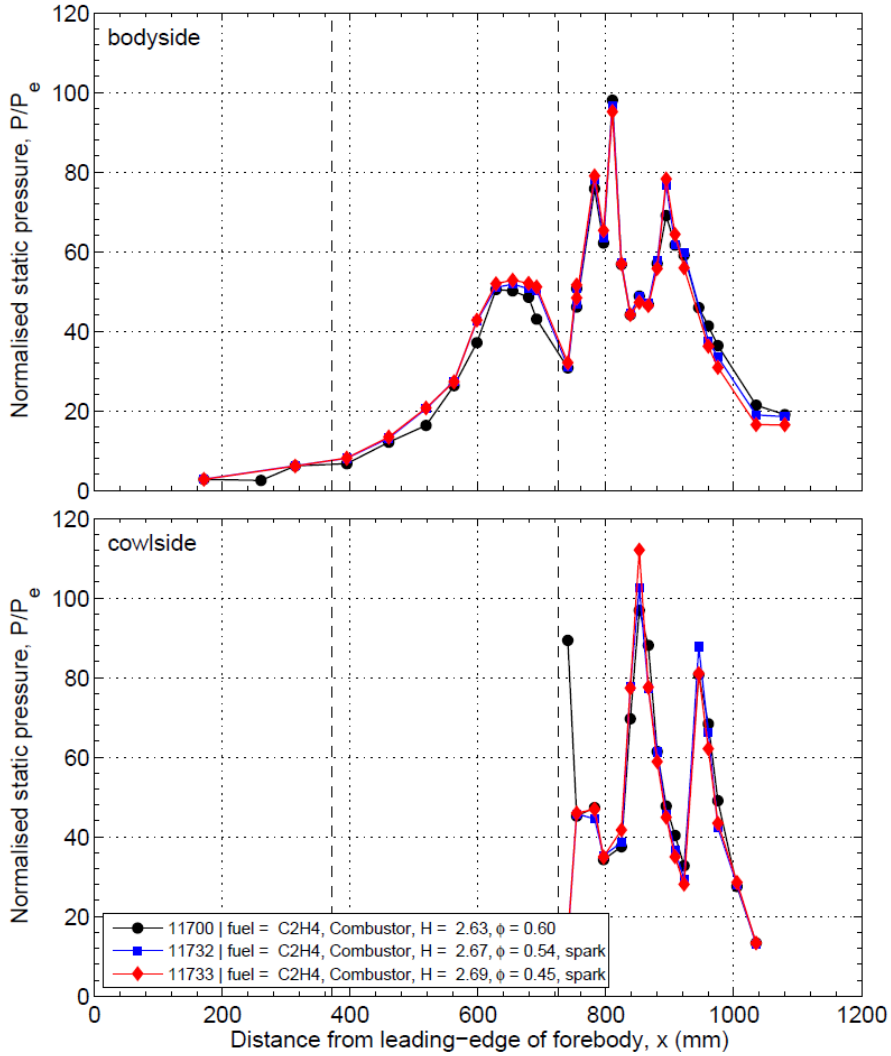

Figure 13: Spark ignition testing of ethylene-air

The spark testing done with gaseous methane still failed to achieve ignition. Similarly, the testing with gaseous ethylene showed a slight increase in pressure rise in the cowl side but no improvement in the body side. This seems to suggest that a sufficiently stoichiometric mixture does not exist in the cavity. CFD simulation results are being pursued to investigate the extent of fuel air mixing within the cavity.

Conclusions

The main objective of this study was to demonstrate the combustion of gaseous hydrocarbon fuels in a "real" engine operating at a high Mach number flight condition. Previous testing with this engine extensively examined the performance of hydrogen fuel. In order to ignite and burn hydrocarbons the combustor was modified to include a cavity flameholder. This series of testing demonstrates that a cavity flameholder promotes the ignition of gaseous ethylene fuel at a flight Mach number of 7.3, with fuel-air equivalence ratios ranging from 0.60-0.70. The results of the current work suggest that the passive entrainment of fuel and air into the cavity sufficiently increases the effective residence time of engine, such that the combustion of ethylene may occur. Spark ignition testing failed to ignite gaseous methane and only showed marginally improved pressure rise for gaseous ethylene.

Future work should focus on improved fuel injection strategies that include injector sizing, including inlet fuelling in combination with combustor fuelling with detailed exploration of equivalence ratios. Hydrogen piloting is another option, albeit adding complexity requiring two fuel-systems on board. The choice of hydrocarbon fuels tested should also be expanded to more realistic jet propulsion fuels or equivalent surrogates.

Technical Outputs

1. Z. J. Denman, S. Brieschenk, A. Veeraragavan, V. Wheatley, M. K. Smart, "Experimental Design of a Cavity Flameholder in a Mach 8 Shape-Transitioning Scramjet", AIAA 2014-2953, AIAA AVIATION 2014 - 19th AIAA International Space Planes and Hypersonic Systems and Technologies Conference, 16 – 20 June, 2014, Atlanta, GA, USA
2. S. Brieschenk, Q. Pontalier, A. Duffaut, Z. J. Denman, A. Veeraragavan, V. Wheatley, M. K. Smart, "Characterization of a spark ignition system for flameholding cavities", AIAA 2014-2242, AIAA AVIATION 2014 - 45th AIAA Plasmadynamics and Lasers Conference, 16 – 20 June, 2014, Atlanta, GA, USA
3. Z. J. Denman, W. Y. K. Chan, S. Brieschenk, A. Veeraragavan, V. Wheatley, M. K. Smart, "Experimental Testing of Hydrocarbons in a Mach 8 Shape-Transitioning Scramjet with a Cavity Flameholder", In preparation to be sent to AIAA J. Propulsion and Power.

References

[1] Lewis, M. J., *Significance of Fuel Selection for Hypersonic Vehicle Range*, Journal of Propulsion and Power, Vol. 17,No. 6, November-December 2001, pp. 1214-1221

[2] Turns, S. R., *An Introduction to Combustion: Concepts and Applications*, McGraw-Hill, 2nd ed., 2000.

[3] Colket, M. B. & Spadaccini, L. J. *Scramjet Fuels Autoignition Study*, Journal of Propulsion and Power, 2001, 17, pp. 315-323

[4] Smart, M. K., "Design of three-dimensional hypersonic inlets with rectangular-to-elliptical shape transition," Journal of Propulsion and Power, Vol. 15, No. 3, 1999, pp. 408- 416

[5] Smart, M.K. and Ruf, E.G., "Free-jet Testing of a REST Scramjet at Off-Design Conditions", AIAA paper 2006-2955, June 2006

[6] Turner, J.C. and Smart, M.K., "Application of inlet injection to a 3-D scramjet at Mach 8", AIAA Journal, Vol. 48, No. 4, pp 829-838, 2010

[7] Gollan, R. J. & Jacobs, P. A. *About Formulation, Verification and Validation of the Hypersonic Flow Solver Eilmer*, International Journal for Numerical Methods in Fluids, 2013, 73, pp. 19-57

[8] G. P. Smith, D. M. Golden, M. Frenklach, N. W. Moriarty, B. Eiteneer, M. Goldenberg, C. T. Bowman, R. K. Hanson, S. Song, W. C. Gardiner, Jr., V. V. Lissianski, and Z. Qin, *GRI-Mech 3.0*, retrieved from http://www.me.berkeley.edu/gri_mech/

[9] R. C. Rogers and C. J. Schexnayder, *Chemical kinetic analysis of hydrogen-air ignition and reaction times*, Tech. rep. National Aeronautics and Space Administration, Hampton, VA (USA). Langley Research Center, 1981.

[10] Tishkoff, J. M., Drummond, J. P., and Edwards, T., *Future Directions of Supersonic Combustion Research Air Force/NASA Workshop on Supersonic Combustion*, Reno, Nevada, 1997.

[11] Ben-Yakar, A. & Hanson, R. K. *Cavity Flame-Holders for Ignition and Flame Stabilization in Scramjets: An Overview*, Journal of Propulsion and Power, 2001, 17, 869-877

[12] Voland, R. T., Auslender, A. H., Smart, M. K., Roudakov, A. S., Semenov, V. L., and Kopchenov, V., *CIAM/NASA Mach 6.5 Scramjet Flight and Ground Test*, 9th International Space Planes and Hypersonic Systems and Technologies Conference, 1999

[13] Gruber, M. R., Baurle, R. A., Mathur, T., and Hsu, K.-Y., *Fundamental Studies of Cavity-Based Flameholder Concepts for Supersonic Combustion*, Journal of Propulsion and Power, Vol. 17, No. 1, January-February 2001, pp. 146-153.

[14] Mathur, T., Gruber, M., Jackson, K., Donbar, J., Donaldson, W., Jackson, T., and Billig, F., *Supersonic Combustion Experiments with a Cavity-Based Fuel Injector*, Journal of Propulsion and Power, Vol. 17, No. 6, November-December 2001, pp. 1305-1312.

[15] Gruber, M. R.; Donbar, J. M.; Carter, C. D. & Hsu, K.-Y. *Mixing and Combustion Studies Using Cavity-Based Flameholder in a Supersonic Flow*, Journal of Propulsion and Power, 2004, 20, pp. 769-778

[16] Davis, D. L. & Bowersox, R. D. W. *Stirred Reactor Analysis of Cavity Flame Holders for Scramjets*, Journal of Propulsion and Power, 33rd Joint Propulsion Conference and Exhibit, 1997, pp. 1-14

[17] Zhang, X., Rona, A., and Edwards, J. A., *The Effect of Trailing Edge Geometry on Cavity Flow Oscillation Driven by a Supersonic Shear Layer*, Aeronautical Journal, Vol. 102, No. 1011, January 1998, pp. 129-136.

[18] Samimy, M., Petrie, H. L., and Addy, A. L., *A Study of Compressible Turbulent Reattaching Free Shear Layers*, AIAA Journal, Vol. 24, No. 2, February 1986, pp. 261-267.

[19] Gruber, M., Smith, S., and Mathur, T., Experimental Characterization of Hydrocarbon-Fueled, Axisymmetric Scramjet Combustor Flowpaths," 17th AIAA International Space Planes and Hypersonic Systems and Technologies Conference, AIAA, San Francisco, California, April 2011, pp. 1-24

[20] Stalker, R. J., Paull, A., Mee, D. J., Morgan, R. G., and Jacobs, P. A., *Scramjets and Shock Tunnels - The Queensland Experience*, Progress in Aerospace Sciences, Vol. 41, No. 6, August 2005, pp. 471-513.

Appendix 1

Milestone Plan

The project includes three activities. Milestones for each are listed below:

Experimental Milestones

1. Cavity Design (July 2013)

Background research on cavity design; determine cavity geometry suitable for the existing engine.

2. Wind tunnel model design and manufacture (December 2013)

Mechanical design of the new cavity based combustor, followed by manufacture and assembly of the engine model.

3. Engine testing (December 2014)

Mach 8 testing of the engine with gaseous hydrogen and gaseous methane fuels.

Computational Milestones

1. One-dimensional combustion simulations (June 2013)

Conduct one-dimensional simulations of stoichiometric, premixed combustion to establish ignition and reaction lengths for hydrogen, methane and ethylene using the GRI-Mech 3.0 mechanism. Validate against existing correlations where available.

2. Axisymmetric premixed simulations (December 2013)

Conduct axisymmetric simulations of stoichiometric, premixed combustion in a cylindrical scramjet combustor followed by expansion through a nozzle. These simulations will account for the effects of boundary layers and shock waves present in the combustor. The specific impulse provided by each fuel will be assessed.

3. Three-dimensional simulations of fuel mixing characteristics (December 2014)

Conduct three-dimensional simulations of fuel injection through a sonic porthole into a supersonic cross-flow at average scramjet combustor conditions. The relative mixing efficiency, jet penetration and stagnation pressure loss for each fuel will be investigated.

Scoping Study Milestones

1. Direct Connect Scoping Study (July 2014)

Study the viability of performing direct connect combustor testing in the T4 shock tunnel, including preliminary estimates of the costs of extra hardware needed to perform this testing.

Appendix 2: Reconfiguration of the T4 Shock Tunnel for Fundamental Scramjet Combustion Testing

Professor Michael K. Smart
Chair of Hypersonic Propulsion
The University of Queensland
m.smart@uq.edu.au

Dr Vince Wheatley
Senior Lecturer
The University of Queensland
v.wheatley@uq.edu.au

Executive Summary

The T4 shock tunnel is a facility designed for generation of true scramjet flight conditions (matching Mach number, velocity and altitude) between Mach 6 and 12. The current test section is configured for free-jet testing of complete scramjet flowpaths (inlet/combustor/nozzle). This report describes a new T4 test section configuration for testing of large scale combustors of any cross-sectional shape in the Mach 6-8 flight regime. It is designed to allow extensive optical access to the combustor using the existing T4 schlieren, chemiluminescence and PLIF systems. It will be ideal for fundamental studies of scramjet ignition, flame-holding and combustion. A budget estimate for the re-configuration is US$198k. The re-configuration can be completed within a period of 6 months.

T4 Shock Tunnel

The T4 free piston shock tunnel facility [1] consists of four main sections; high pressure reservoir, compression tube, shock tube and test-section, as shown in Figure 1. A shock wave generated in the test gas contained in the shock tube increases its pressure and temperature. Reflection of the shock wave from the end of the shock tube stagnates the test gas, which subsequently expands through the nozzle producing a high-speed test flow of several milliseconds duration. This process allows the high stagnation enthalpies characteristic of hypersonic flight to be reproduced, which is of primary importance in combustion experiments.

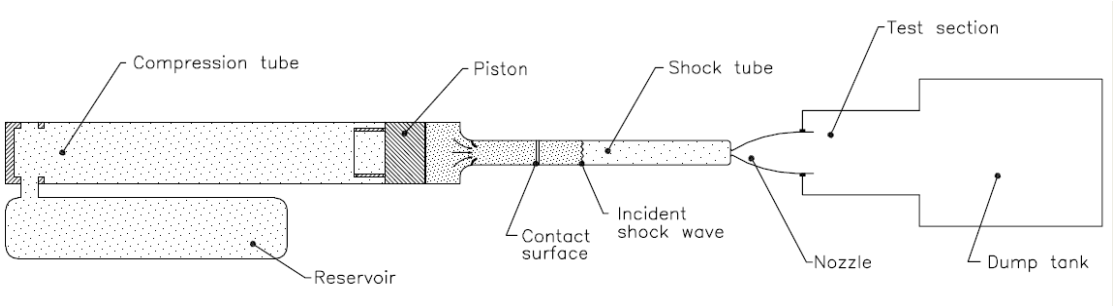

Figure 1 - Components of the T4 reflected shock tunnel

The current T4 test section is configured for free-jet testing of complete flowpaths (inlet/combustor/nozzle) as shown in Fig. 2. In this instance the flow exiting the facility nozzle is equivalent to the flight conditions. In some cases semi-free-jet testing is done, where the flow exiting the facility nozzle is equivalent to that on the forebody of a vehicle. This report details a re-configuration of the T4 test section for fundamental studies of scramjet combustors.

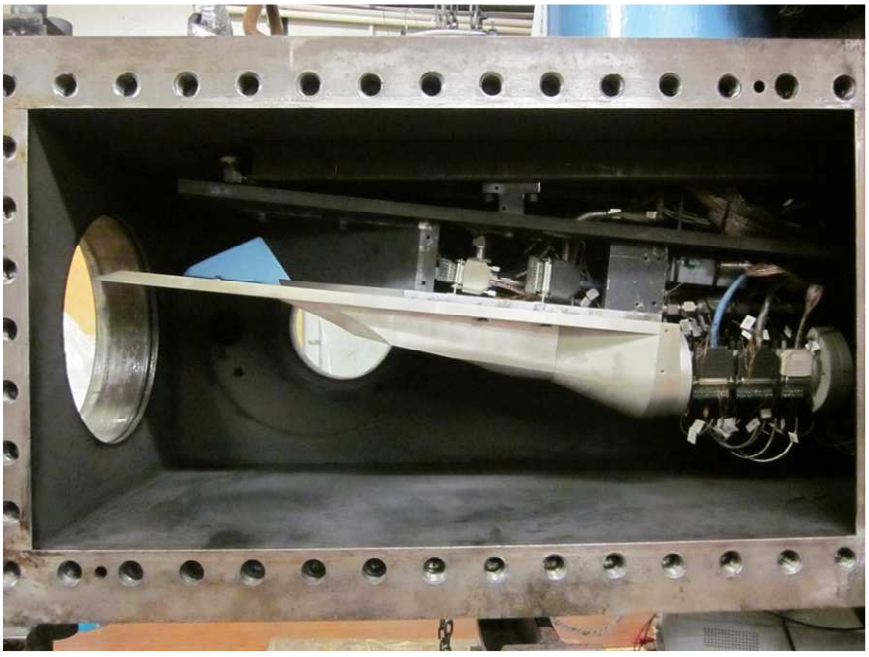

Figure 2 - Full flowpath scramjet model in existing T4 test-section

Fundamental Combustion Testing in T4

There is a desire to conduct fundamental investigations of combustion and flame-holding phenomena in scramjet combustors in the Mach 6-8 flight regime. These investigations are best performed with a uniform inflow to the combustor in order to simplify interpretation of experimental results and corresponding computational simulations. Two test techniques are typically used to perform these types of experiments:

1. Direct connect experiments, where the combustor connects directly to the exit of the facility nozzle. This configuration has the advantage of using all the flow generated by the facility, but has the limitation that the cross-section of the combustor entrance must be the same as the exit of the facility nozzle. The combustor must also ingest the facility boundary layers.
2. Cookie-cutter experiments, where the combustor entrance is placed within the core flow of the facility nozzle thus capturing only a portion of the facility test flow. This configuration has the advantage of being able to test many different combustor shapes (axi-symmetric, rectangular, square etc), and allows uniform flow to enter the test article.

It is proposed here to re-configure the T4 facility test section to enable cookie-cutter experiments. This configuration will allow many different combustor configurations to be examined. Despite the fact that this technique does not use all the flow generated by the facility, the large size of the T4 facility means that realistic scale combustors can be tested.

Proposed Re-configuration of the T4 Test Section

A schematic of the re-configured test section is shown in Figure 3. Entering from the left is the existing shock tube and a new Mach 6 contoured nozzle. The dark-grey tank is the proposed new test section. This has been designed to contain both free-jet experiments as well as the proposed fundamental combustor experiments. The new test section has been designed with significantly enhanced optical access from the sides, top and bottom. Access to the model will be through the side doors that will open on hinges, and the existing T4 amplifier banks (not shown) will be installed above the existing dump tanks (shown in red in Fig. 3). The existing fuel system will also be unchanged.

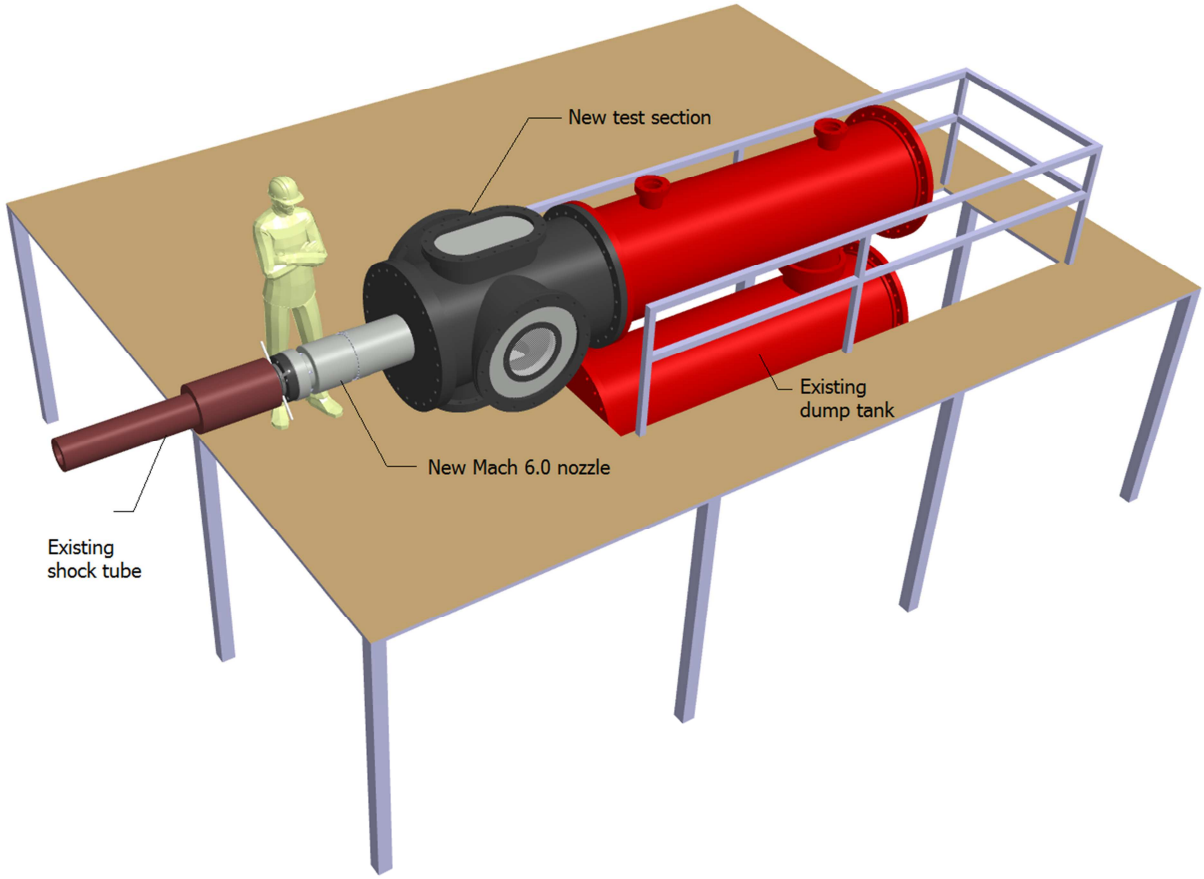

Figure 3 - Schematic of proposed T4 re-configuration

A typical combustion experiment that could be performed in the new test section configuration is shown in Figures 4 and 5. This experiment is designed to examine hydrocarbon combustion and flame-holding at Mach 7 flight conditions. A Mach 6 facility nozzle would be used to produce a 200 mm (~7.9 in) diameter core flow. A set of 2-D wedges would be set-up within the core flow to shock it down from Mach 6 to a desired Mach 3 flow entering the combustor. A rectangular duct with an entrance height of H = 36 mm (~1.4 in) and an entrance width of W = 100 mm (~3.9 in) captures a portion of the uniform Mach 3 flow. Note that the boundary layers formed on the wedges and the side-plates that support them do not enter the duct, nor do the shocks generated by the wedges. A typical set of flame-holding cavities on the top and bottom of the duct are shown, and the combustor diverges to allow fuelling at high equivalence ratio.

Flow phenomena in the combustion duct can be visualised using schlieren, chemiluminescence and PLIF. This will be in combination with pressure and heat transfer measurement. The two side doors contain 350 mm (~13.8 in) diameter glass windows to allow a large view of the combusting flow using the existing T4 schlieren and chemiluminescence systems. The field-of-view allowed by these windows is shown in Figure 6. Optical diagnostics such as PLIF require high quality Fused Silica (or equivalent) windows that would be prohibitively expensive at this size. It is proposed to purchase 190 mm (~ 7.5 in) diameter Fused Silica windows for the two sides and top, that will be inset within metallic blanks. These can be used to visualise the combusting flow using the existing T4 PLIF system. The experimental model would also require two Fused Silica windows on its sides, and a small Fused Silica insert in the top of the model for the light sheet (not shown in the Figures).

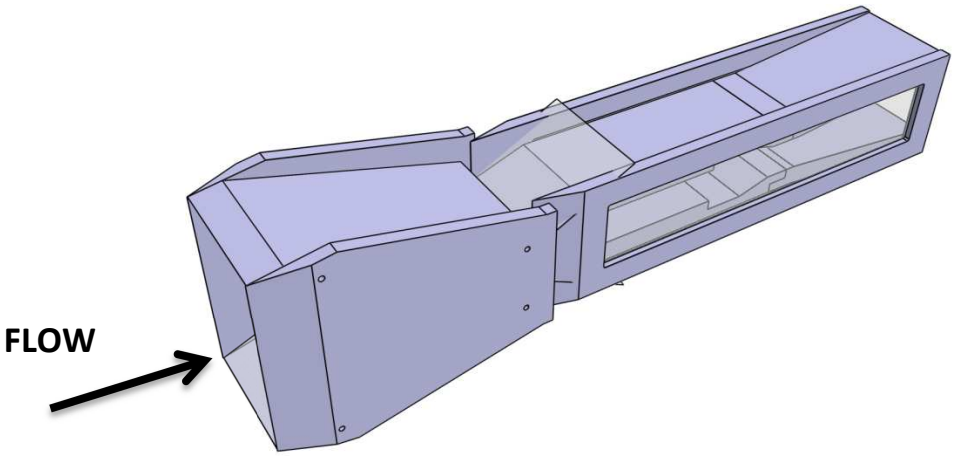

Figure 4 – Schematic of fundamental combustion experiment hardware

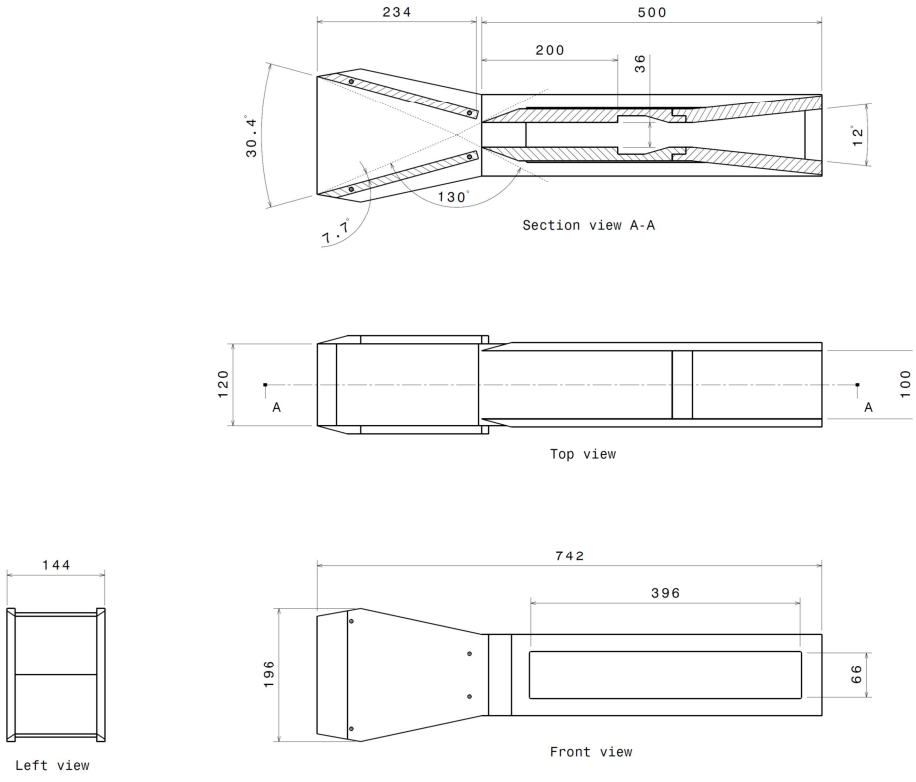

Figure 5 – 3 Views and a section of fundamental combustion experiment hardware

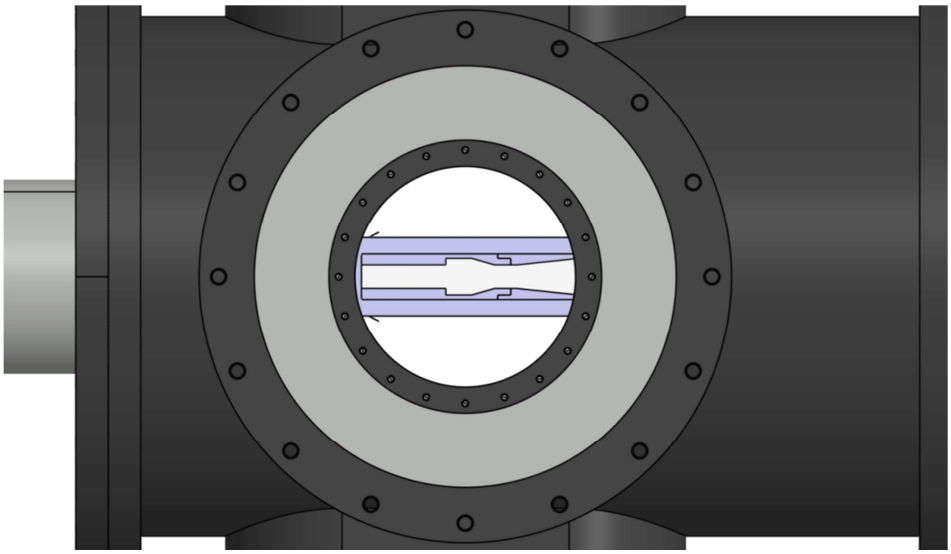

Figure 6 – Typical field-of-view for schlieren and chemiluminescence system.

Budget

A budget estimate has been prepared based on the proposed test section re-configuration. The total cost to manufacture and install the new test section and the experimental model is US$198k. An exchange rate of AU$ = 0.95$US has been used for this estimate. The hardware can be manufactured and installed within a period of 6 months from the time when resources are received.

The cost breakdown is as follows:

Item	Cost (US$)
Test Section Vessel (including design, manufacture, hydro testing and qualification)	70,000
Mach 6 axi-symmetric contoured nozzle	18,000
Structural Support of test section	10,000
Installation (Mechanical Technician – 400 hrs)	28,000
2 x Schlieren Windows (350mm diameter glass)	5,000
3 x PLIF windows (190 mm Quartz)	8,000
“cookie-cutter” experimental model	35,000
2 x PLIF windows in model (Quartz)	8,000
Kulite pressure instrumentation (10)	16,000
Total	198,000

Note that these costs are for hardware only. They do not include the costs of using the facility. This will be detailed in a separate document.

Summary

The hardware modifications described in this report will enable fundamental combustion studies to be performed in T4 in the Mach 6-8 flight range.

References

[1] Stalker, R. J., Paull, A., Mee, D. J., Morgan, R. G., Jacobs, P. A., “Scramjets and shock tunnels – the Queensland experience,” Progress in Aerospace Sciences, Vol. 41, No. 6, 2005, pp. 471-513.

Appendix 3: AIAA – Journal of Propulsion and Power Manuscript Draft

Experimental Testing of Hydrocarbons in a Mach 8 Shape-Transitioning Scramjet with a Cavity Flameholder

Zachary J. Denman[a], Wilson Y. K. Chan[b], Stefan Brieschenk[b],

Ananthanarayanan Veeraragavan[c], Vincent Wheatley[d] and Michael K. Smart[e]
University of Queensland, Brisbane, Queensland 4072, Australia

The design and testing of a cavity flameholder in a Mach 8 rectangular-to-elliptical shape-transitioning scramjet is presented. The experimental results presented are from the shock tunnel testing of the engine, fitted with the cavity combustor and fueled by gaseous ethylene, methane, and hydrogen. Axisymmetric simulations of a cavity in a diverging combustor were used to confirm that the cavity flow would fully establish in the limited test time available in this impulse facility. The cavity flameholder was designed such that autoignition and flameholding of gaseous ethylene-air mixtures should occur. Successful combustion and flameholding of ethylene and hydrogen was observed at a flight Mach number of 7.3 and and dynamic pressure of 53.5 kPa. Methane did no ignite at any of the conditions tested. Static pressure measurements were taken along the entire flowpath of engine. The engine was fueled at equivalence ratio ranging from $0.6 < \phi < 0.7$.

[a] Ph.D. Candidate, Centre for Hypersonics, School of Mechanical and Mining Engineering, Student Member
[b] Postdoctoral Research Fellow, Centre for Hypersonics, School of Mechanical and Mining Engineering, Member
[c] Lecturer, Centre for Hypersonics, School of Mechanical and Mining Engineering, Member
[d] Senior Lecturer, Centre for Hypersonics, School of Mechanical and Mining Engineering, University of Queensland, Senior Member
[e] Professor, Centre for Hypersonics, School of Mechanical and Mining Engineering, Senior Member

Nomenclature

$A,\ a,\ b$ = Empirically determined coefficients for ignition delay correlation

D = Cavity depth, mm

E = Parameter equivalent to global activation energy, cal/mol

h = Altitude, km

H = Enthalphy, J/kg

L = Cavity length, mm

M = Mach number

p = Static pressure, Pa

q = Dynamic pressure, Pa

R_u = Universal gas constant, cal/mol/K

T = Temperature, K

u = Velocity, m/s

x = Distance from forebody tip, projected along combustor axis, m

y^+ = Dimensionless wall distance

Subscripts

avg = Average property within cavity

$core$ = Core property within cavity

e = Nozzle (facility) exit condition

f = Flight condition

s = Nozzle (facility) supply property

$wall$ = Wall property

∞ = Freestream property

Greek Letters

θ = Aft-wall angle of cavity, degrees

ϕ = Fuel-air equivalence ratio

τ_r = Residence time of cavity flameholder, s

τ_{ign} = Ignition delay time, s

γ = Ratio of specific heats

I. Introduction

Supersonic combusting ramjets (scramjets) show great potential as airbreathing alternatives to rocket-based access-to-space system stages [1]. Research into combined rocket-scramjet-rocket systems has shown that these vehicles would have the ability to launch small payloads (200 kg) into low Earth orbit [2, 3], drastically reducing launch costs and potentitally increasing the number of launches.

Over the past forty years, it has been accepted that a useable scramjet engine will, most likely, be highly integrated into the airframe of the vehicle it is propelling [4]. This airframe-integration, however, places considerable volume constraints on the supporting systems such as the fuel systems. Hydrogen has typically been the fuel of choice for scramjets due to its favourable ignition characteristics and high specific energy. However, hydrogen suffers from low energy density, which necessitates examining fuels with high energy densities, namely hydrocarbon fuels. Figure 1 clearly shows the benefits of using a low-order hydrocarbon fuel, such as ethylene or methane, over hydrogen from an energy per volume standpoint.

While hydrocarbon fuels are appealing due to their higher energy density and favourable handling characteristics, their longer ignition time pose a significant problem due to the extremely short flow residence times (on the order of one millisecond) in scramjet-powered vehicles above Mach 7. In order to make use of hydrocarbon fuels, piloting and flameholding sites may need to be established within the engine [7]. Cavity flameholders, such as the one shown in Fig. 2, have been proposed as a promising means by which ignition and flameholding of low-order hydrocarbons may be achieved in supersonic combustors [8].

Ben-Yakar and Hanson completed an in-depth overview of the literature on cavities and the various parameters that govern their performance [9]. This summary of research efforts indicates that there appears to be optimal dimensions for cavities to act as flameholding devices depending on the flow regime the cavity is operating. Generally, open cavities ($L/D <$ 7-10) are preferred for flameholding applications as they exhibit lower drag penalties when compared to closed cavities [9]. The dimensions of the cavity, such as depth and aft wall angle, must be determined based on the required residence time of the cavity; which in turn is set by the selected fuel. Davis and Bowersox give an equation for calculating the cavity depth required for a given residence time [10, 11]. This expression is shown in Equation 1. Davis and Bowersox's equation is based on the assumption that the flow in the cavity is perfectly stirred (uniform species and temperature distribution).

$$D = \frac{\tau_r U_\infty}{40} \tag{1}$$

The cavity must provide sufficient residence time such that the combustible mixture has time to ignite. An appropriate method for determining this time is through ignition delay formulas, such as those proposed by Colket and Spadaccini [12]. The ignition delay formula is shown in Equation 2.

$$\tau_{ign} = A \exp\left(\frac{E}{R_u T}\right) [O_2]^a [C_x H_y]^b \tag{2}$$

Coefficients for hydrogen, ethylene and methane are shown in Table 1. Using Eq. 1 and 2 (as well

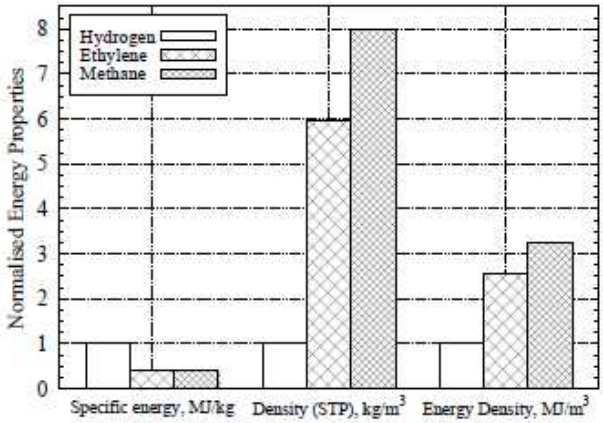

Fig. 1 Properties of candidate scramjet fuels, normalized by properties of hydrogen. Hydrogen specific energy, density (STP), and energy density are 120 MJ/kg, 71 kg/m^3, and 8300 MJ/kg respectively. [5, 6]

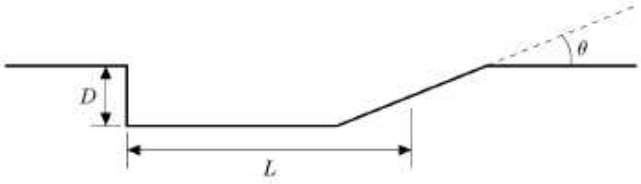

Fig. 2 Schematic of cavity flameholder

as an assumed temperature and pressure within the cavity), an estimate for the cavity depth can be obtained by setting τ_r equal to τ_{ign}.

Table 1 Ignition delay formula coefficients for fuels considered [12]

Fuel	A	E (kcal/mole)	a	b
Methane	2.21×10^{-14}	45,000	−1.05	0.33
Ethylene	2.82×10^{-17}	35,000	−1.20	0.00
Hydrogen	1.60×10^{-14}	19,700	−1.00	0.00

For cavities to act as flameholders, a stable flowfield in the cavity is desirable. At the Air Force Research Laboratory (AFRL), Gruber *et al.* demonstrated that this can achieved by reducing the aft wall angle, θ, below 90°; this however, resulted in increased drag and reduced residence time [13]. Ben-Yakar and Hanson also surveyed works by Zhang *et al.* and Samimy *et al.* in regards to the optimal aft wall angle [14, 15]. A comparison of these works suggests that there is an optimal aft wall angle between 16° and 45°.

An extensive research program conducted by the AFRL has shown that cavity flameholders can sustain the combustion of low-order hydrocarbon fuels, such as ethylene, at supersonic flow conditions [13, 17, 18]. More recently, the AFRL performed experiments with annular cavities in axisymmetric combustors at simulated flight conditions between Mach 3 and 5 [19]. Combustion of heated ethylene was successfully sustained over a wide range of fuel equivalence ratios ($0.2 < \phi < 1.0$) using cavity fueling when required.

This paper documents a series of experiments that were carried out in the T4 Reflected Shock Tunnel at the University of Queensland. Previous shock tunnel testing has examined the 75%-scale HIFiRE 7 engine with hydrogen [24]. This flowpath has been been modified to include a cavity

flameholder so that testing with hydrocarbon fuels may be completed. These tests experimentally investigate the combustion of low-order hydrocarbons (ethylene and methane), as well as hydrogen, in a Mach 8 shape-transitioning scramjet engine. This engine is a practical engine geometry which may easily be integrated into the airframe of a vehicle. The shape-transitioning inlet generates a non-uniform inflow for an elliptical combustor; rather than a circular or planar combustor. Static pressure measurements taken throughout the flowpath are presented.

Following the Introduction, this paper outlines the methodology used in designing the cavity flameholder that was included in the engine flowpath. Next, the paper presents the details of the experimental model, as well as a description of the experimental facility and test conditions. Details of the fuel system are also presented along with the data reduction process. Finally, results of the experiments are presented.

II. Design of a cavity for low-order hydrocarbon fuel flameholding in Mach 8 REST engine

Previous testing of a cavity with an L/D ratio of 4.0 and an aft-wall angle (θ) of 22.5 degrees was performed at the AFRL [17, 18]. These cavity dimensions lie within the open cavity regime, as well as the range for a cavity with a stable flowfield and minimum drag. As the depth of the cavity is proportional to the residence time of the cavity, Davis and Bowersox's relation for cavity depth (Equation 1) [10] coupled with Colket and Spadaccini's ignition delay time correlation (Equation 2) [12], may be used to estimate the required depth of the cavity for autoignition of the chosen fuel.

As the ignition delay time of a combustible mixture is highly dependent on temperature, the temperature within the cavity must first be estimated. These simulations were also used to determine if the cavity flow establishes in a sufficiently short time, such that impulse testing will yield meaningful results. This was done using axisymmetric RANS simulations in the University of Queensland's hypersonic flow solver, Eilmer3 [20]. A nominal cavity depth of 4.4 mm was simulated; this cavity has an identical depth to combustor hydraulic diameter ratio as a previously tested cavity [18, 19]. The simulations used the $k-\omega$ turbulence model and assumed a thermally perfect gas. In the simulations, the combustor is initially filled with low pressure quiescent air with a temperature of 300 K and a pressure of 66.5 Pa to match the conditions in the test section of the facility prior to the arrival of the test flow. A supersonic inflow boundary condition on the inlet of the domain

Table 2 Inflow conditions for cavity simulations extracted from the Mach 8 REST combustor entrance [21]

Temperature (K)	Pressure (kPa)	Velocity (m/s)
932	47.9	2005

supplies the flow state expected at the Mach 8 REST combustor entrance (flow conditions shown in Table 2). The pressure difference between the inflow boundary and the initial fill gas drives a strong shock wave through the combustor, mimicking the shock tunnel start-up process. The inflow turbulence intensity and laminar-to-turbulent viscosity ratios were 0.01 and 1.0, respectively. The turbulent Prandtl and Schmidt numbers were set to 0.89 and 0.75, respectively. The grid was refined to a point where the centers of the cells adjacent to walls had y^+ less than one. A fixed temperature boundary condition ($T_{wall} = 300$ K) was used along all combustor surfaces, corresponding to testing in an impulse facility, and an extrapolation boundary condition was applied at the outflow.

Simulations were run on a 29,200 cell base grid. To evaluate the adequacy of this resolution, the reference simulation was repeated with grid refinement ratios of 3/2 and 2. The convergence of the average outflow static temperature and streamwise momentum flux were examined using generalised Richardson extrapolation for unequal refinement ratios, as detailed in [22]. The order of convergence of these statistics was two in both cases, with the convergence being monotonic. For the simulation on the fine grid, the average static temperature and momentum flux differ from their Richardson extrapolated values by -0.2% and 1.9%, respectively. This demonstrates that the effect of discretisation error on the solution is acceptably small. Figure 3 shows the temperature profile at various points within the cavity. The profiles for the base, medium, and fine grids are shown at three locations. There is very good agreement between the medium and fine grids at all locations. This indicates that the domain is sufficiently resolved by the medium grid. Simulations were run for 0.5 ms of flow time. At this point, the maximum volume-weighted ℓ^2 norm of temperature and pressure across the domain vary by 0.02% and 0.08% of the freestream properties, for the medium grid.

Figure 4 shows the temperature contours of the flow within the cavity at various times through-

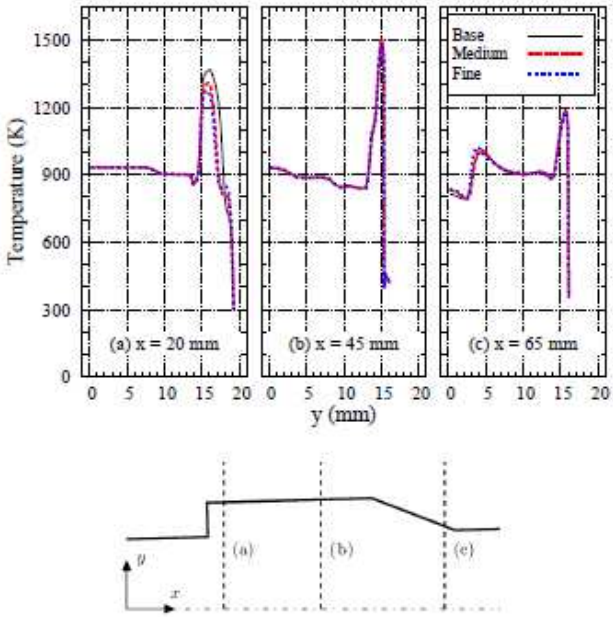

Fig. 3 Temperature profile at different axial locations throughout axisymmetric cavity flameholder

out the simulation; the full domain is 200 mm long. The temperature and pressure (mass-weighted) in the "core" of the cavity are 1490 K and 37.1 kPa, respectively. The "core" temperature of the cavity was determined by excluding temperatures in the thermal boundary layer that were below the average temperature (T_{avg} = 1290 K) of the flow within the cavity. Comparison of Fig. 4d and 4e shows that the cavity flowfield is well established by 150 μs. Over the next 150 μs (Fig. 4f), the flow behind the rearward facing step is further heated, but the overall flowfield within the cavity is relatively unchanged. The core temperature within the cavity was used to estimate the ignition delay time for ethylene, methane, and hydrogen in the engine.

Figure 5 shows the residence time of a cavity as a function of cavity depth using Eq. 1 and 2. Davis and Bowersox's relation divides the domain into two regions; flameholding and non-flameholding. The ignition delay times of hydrogen and ethylene (at the cavity core temperature and pressure) are shown as horizontal lines; the ignition delay time of methane is approximately 2 ms at the core temperature and pressure, which is too long for the experimental model and suggests forced ignition is necessary for methane. The intersection of these lines and Davis and Bowersox's relation, indicates the minimum depth required for an auto-igniting cavity for that fuel, at the con-

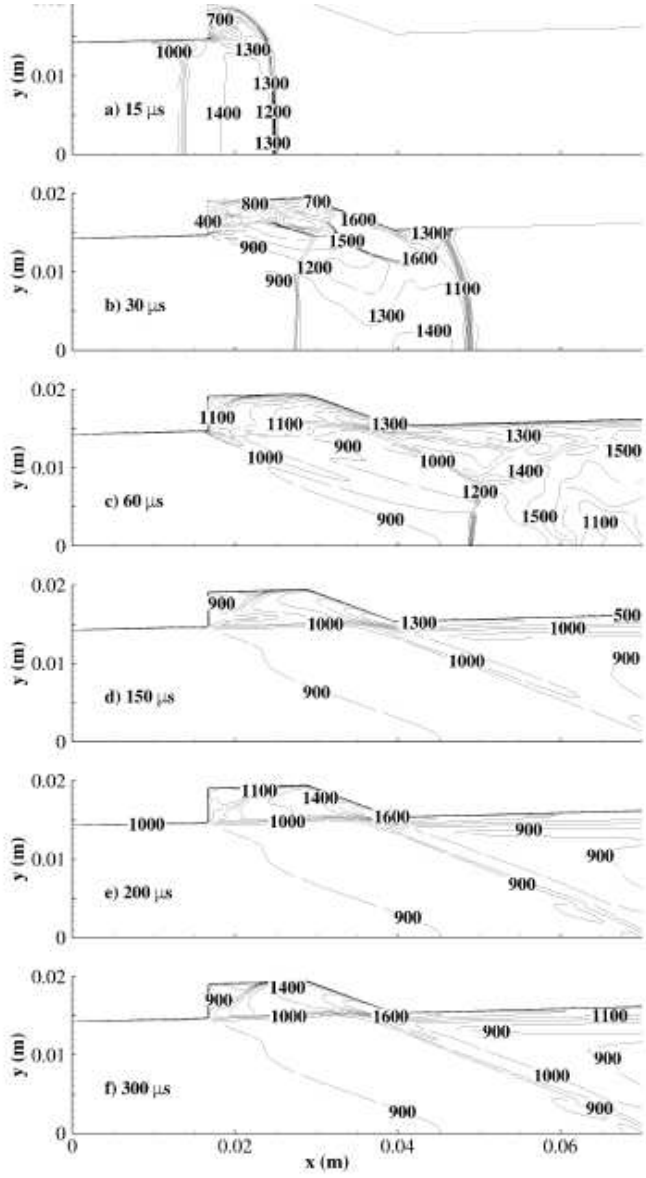

Fig. 4 Temperature contours in an axisymmetric, unfueled, simulation of cavity flameholder in diverging combustor at various times

ditions noted. The minimum depth required for a cavity that will auto-ignite ethylene, based on the temperature and pressure in the cavity from the axisymmetric simulations, is approximately 4 mm. Using this design methodology, a cavity depth of 100 mm is required for methane, at the core temperature and pressure, which is far too large to be incorporated into the engine geometry.

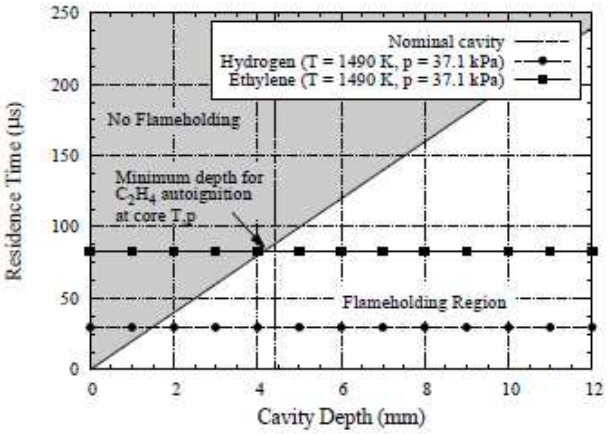

Fig. 5 Depth of cavity based on Davis and Bowersox relation, coupled with Colket and Spadaccini's ignition delay correlations for hydrogen and ethylene with $\phi = 0.7$

III. Experimental Model

A schematic of the scramjet engine tested is provided in Fig. 6. The experimental model is approximately 1100 mm long and 150 mm wide. The model has four main components; a steel forebody, a Mach 8 REST inlet, a combustor with cavity flameholder, and nozzle. During testing the model is inclined at 6° to the incoming flow to allow for freejet testing [23, 24]. The REST inlet has an overall geometric contraction ratio of 5.80 and an internal contraction ratio of 1.99. A constant-area section, 110 mm long is included as part of the inlet. The combustor and nozzle are 229 mm and 150 mm in length, and diverge uniformly with area ratios of 2.0 and 2.5, respectively.

The cavity flameholder described in Section II can be seen, along with spark plugs, on the top (bodyside) and bottom (cowlside) of the engine, which are in place for a later study. Fuel can be injected on the inlet through three equispaced 1.613 mm diameter porthole injectors or at the combustor entrance through eight equispaced 1.041 mm diameter porthole injectors. All injectors are inclined at 45° to the local flow direction. This paper presents results from combustor-only fueled experiments. Figure 7 shows the experimental model mounted in the test section of the T4 Reflected Shock Tunnel.

The static pressure along the flowpath and in the fuel plenums is measured by 52 Kulite® XTEL-190 (M) piezo-resistive pressure transducers. The temperature of the injected fuel was also measured using an Omega® CHAL-003-BW thermocouple located in the fuel plenum. A "sawtooth"

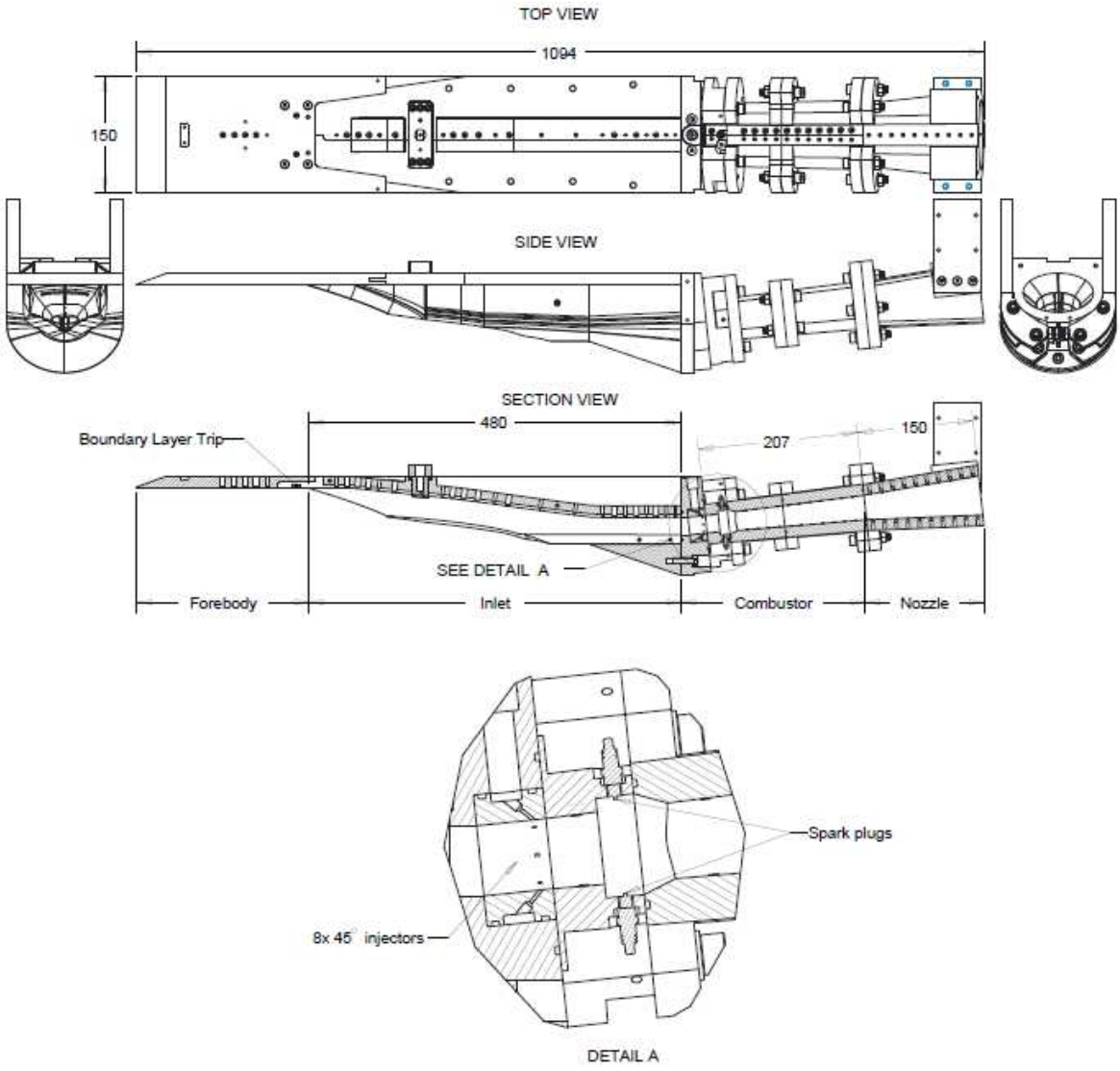

Fig. 6 Schematic of experimental model

boundary layer trip was installed on the model, 10 mm upstream of the inlet entrance for all tests. The sawtooth trip is a saw blade which has been bent 90°. Further details of the boundary layer trip are outlined in previous works [24].

(a) Side view

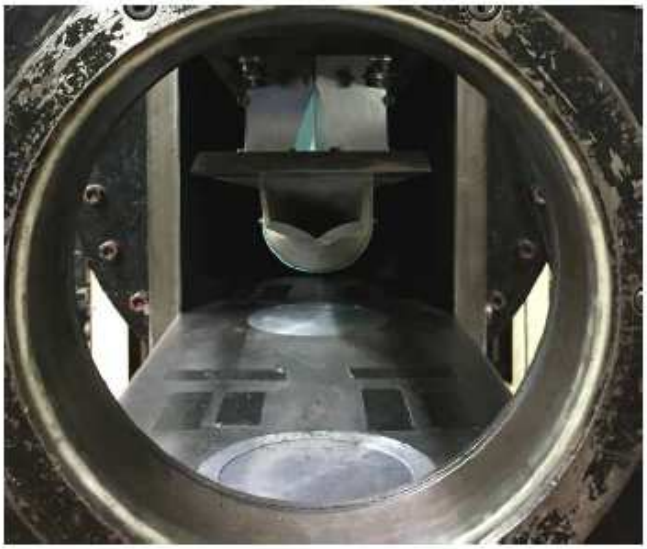

(b) Front view

Fig. 7 Experimental model in test section

IV. Test and Fueling Conditions

The experiments were conducted in the T4 Reflected Shock Tunnel at the University of Queensland [25]. The T4 Reflected Shock Tunnel is a free-piston driven shock tunnel, where high pressure air is used to accelerate a piston along the driver tube, compressing the driver gases, which then ruptures a mild steel diaphragm (of varying thicknesses). A shock then propagates along the shock tube, heating and compressing the test gas. This shock is reflected at the end of the shock tube, further heating and compressing the test gas, just upstream of the facility nozzle, where a mylar diaphragm is then ruptured. The high pressure and temperature gas is then expanded through a converging-diverging nozzle and passes over the model, located in the test section. The choice of

Table 3 Nominal experimental and flight conditions

Nozzle-supply conditions			Derived freestream conditions					Flight conditions		
p_s	T_s	H_s	p_e	T_e	u_e	M_e	γ_e	M_f	h_f	q_f
MPa	K	MJ/kg	kPa	K	m/s	–	–	–	km	kPa
20.8	2500	2.65	1900	231	2330	7.64	1.40	7.32	28.7	53.5

nozzle determines the Mach number in the test section.

The outflow of the Mach 7.6 facility nozzle was examined via a pitot survey prior to the actual experiments, to ensure that the facility nozzle is providing a uniform region of flow at the inlet of the engine. All experiments were performed using the nominal test conditions shown in Table 3. The test conditions correspond to a Mach 7.3 flight condition at an altitude of 28.7 km with a dynamic pressure of 53.5 kPa. As the experimental model is a 75%-scale of a flight model, Reynolds number scaling was used in the estimation of the equivalent flight conditions. The properties of the flow exiting the facility nozzle are estimated using the ESTCj code [26].

Data is collected using a National Instruments (NI) PXI-8196 Controller (mounted in a NI PXI-1045 chassis), with 13 NI PXI-6133 data acquisition cards, connected to a Windows workstation. This system is capable of recording 104 analog output channels at up to 2.5 MS/s. A LabVIEW Virtual Instrument (VI) controls the data acquisition system and is responsible for the triggering of the fast-acting solenoid valve used to control the flow of fuel into the engine from a Ludweig tube. This valve must be triggered prior to arrival of the test flow in order to have a near-constant fuel flow rate during the test.

Figure 8 shows the fuel plenum traces for hydrogen and ethylene for the same Ludwieg tube fill pressure. Hydrogen reaches a steady plenum pressure in approximately 10 ms, whereas ethylene takes approximately 30 ms. Due to this difference, more fuel is present inside the engine prior to the arrival of test flow. Previous testing has shown that this fuel can alter the behaviour of the engine for ethylene-fueled experiments. Hydrogen-fueled experiments were not affected by the amount of fuel present in the engine prior to the test. Therefore, the amount of pre-fueling conducted prior to an ethylene-fueled experiment must be limited; this results in a rising plenum pressure during the

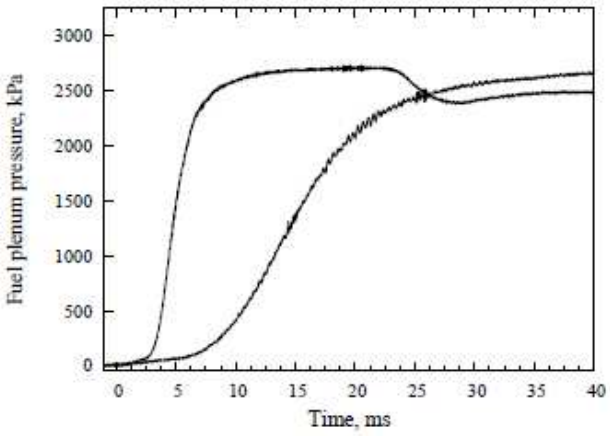

Fig. 8 Fuel injection timing relative to test time

test time.

V. Data Reduction

Figure 9 shows typical static pressure measurements recorded by the T4 data acquisition system during an experiment. The Mach 7.6 facility nozzle takes approximately 0.75 ms to start-up, indicated by region (a) in Fig. 9. Following the nozzle start-up process, the flow inside the engine is assumed to establish within approximately three flow lengths [27]. For the current model, this is approximately 1.2 ms and is represented in Fig. 9 by region (b). The cavity flow should easily be established in this time, based on the results of the transient simulations presented in Section II. The test time (viz. the time over which data is averaged for a test) begins after flow has established in both the Mach 7.6 nozzle and the experimental model, and ends 0.5 ms later. The test time is indicated by region (c) in Fig. 9. The end of the test time is chosen prior to the test flow becoming contaminated with driver gas.

VI. Results and Discussions

The following section will outline the results of the experiments. The discussions in this section will be limited to the combustor-only fueled experiments. Firstly, the inclusion of a cavity flameholder will be examined, followed by fuel-off and suppressed-combustion experiments. After this, the ethylene-fueled experiments will be discussed. Finally, the performance of hydrogen, ethylene, and methane fuels will be compared.

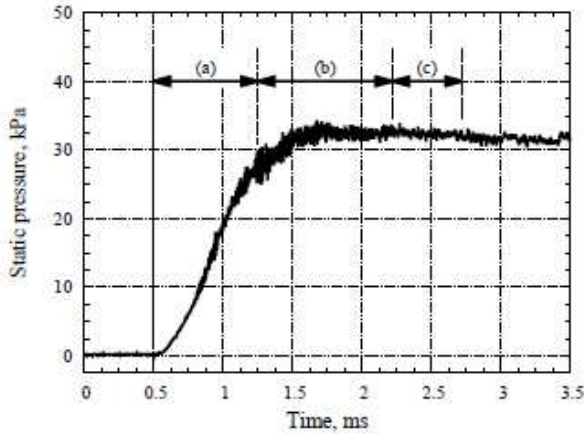

Fig. 9 Typical static pressure trace from Kulite® XTEL-190 (M) recorded through T4 data acquisition system (shot 11714)

In the plots of pressure distribution in the following sections, a schematic of the engine is shown above all plots with the combustor injection location ($x = 725$ mm) shown by a vertical dashed line. All pressure measurements have been normalized by the freestream pressure (viz. facility nozzle-exit pressure), p_e corresponding to each test.

A. Fuel-off experiments with and without cavity flameholder

Previous testing with this engine, without a cavity flameholder has been performed. With the inclusion of a cavity flameholder at the beginning of the combustor, it is important to establish a new baseline measurement for the pressure within the flowpath. Figure 10 shows results from previous testing without a cavity flameholder (shot 11413) and the current testing with a cavity (shot 11692).

The pressure distributions for both shots in Fig. 10 along the bodyside of the inlet match very closely. These experiments were performed nearly fifteen months apart and the agreement shown in these traces provides a good indication that the integration of the experimental model into facility has been performed in a consistent manner. The distributions have been truncated at the combustor exit due to the two experiments having used different thrust nozzles. The most noticeable difference between the two pressure distributions is the large secondary peak (RB2b) that occurs on the bodyside of the engine at $x = 810$ mm with the introduction of the cavity flameholder. As the smaller upstream peak, at $x = 782$ mm, is present in both experiments in Fig. 10, it is most

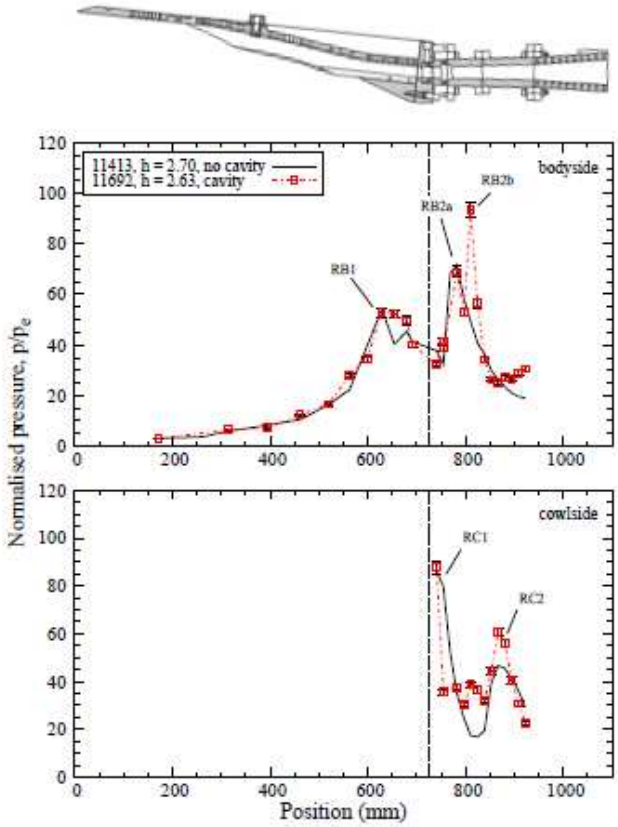

Fig. 10 Fuel-off comparison, with and without cavity flameholder

likely the second reflection shock of the cowl shock on the bodyside of the engine, indicated by RB2a. This new, larger peak (RB2b), can therefore, be associated with the inclusion of the cavity flameholder in the combustor. The cavity flameholder generates a strong recompression shock from its aft-wall; this spike in pressure is, very likely, caused by this shock. Downstream of this shock, the pressure recovers to approximately the same level as in the experiment with no cavity. Changes to the pressure distributions are also evident on the cowl side of the engine. The large spike in pressure (RC1) is still present just downstream of the injection location. The drop from this high level occurs earlier compared to previous tests without the cavity due to the fact that transducer located at $x = 754$ mm is within the cavity, that is, behind a rearward facing step.

B. Ethylene-fueled experiments

The results of the ethylene-fueled experiments are shown in Fig. 11. Ignition and combustion of ethylene was achieved for all equivalence ratios tested. Pressure distributions from three fuel-on experiments at varying equivalence ratio are shown (shots 11697, 11698 and 11700) with an

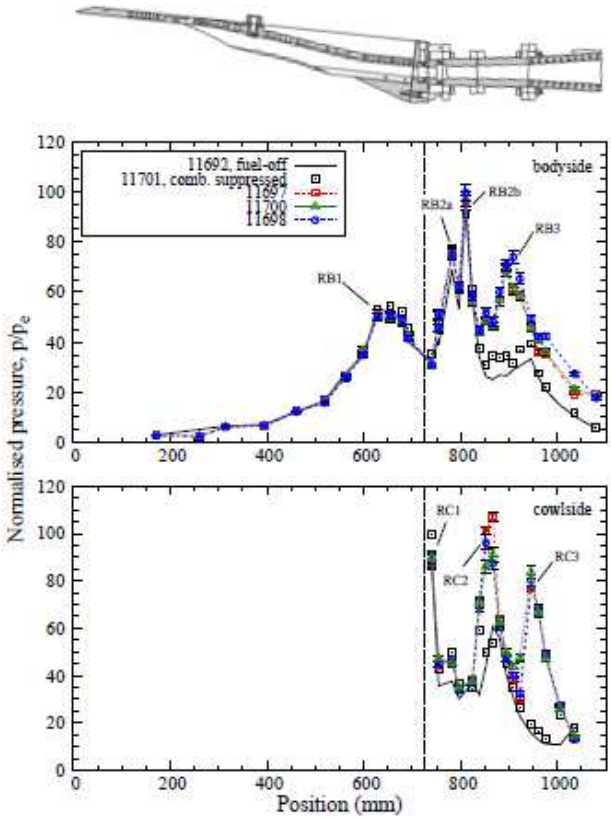

Fig. 11 Ethylene-fueled experiments

experiment where combustion was suppressed (shot 11701) by using a nitrogen test gas, instead of air. The pressure distributions in Fig. 11 clearly show an increase from a combustion-induced pressure rise from $x = 850$ mm to the nozzle exit, when compared to the combustion-suppressed shot. This increase is evident in both the bodyside and cowlside pressure distributions. The pressure rise occurs approximately 90 mm downstream of the cavity. It is possible that the flow is ignited by the recompression shock downstream of the cavity.

A marginally higher pressure is seen at a majority of sensor locations in the pressure distribution corresponding to a higher equivalence ratio (shot 11698). Peak pressures on the bodyside are relatively unaffected by equivalence ratio, but the pressure rise is maintained further downstream. The spikes in the pressure distribution on the cowlside of the engine indicate the flowfield to be shock-dominated. However, both sides of the engine show the aforementioned pressure rise for the fuel-into-air shots over the combustion-suppressed shots.

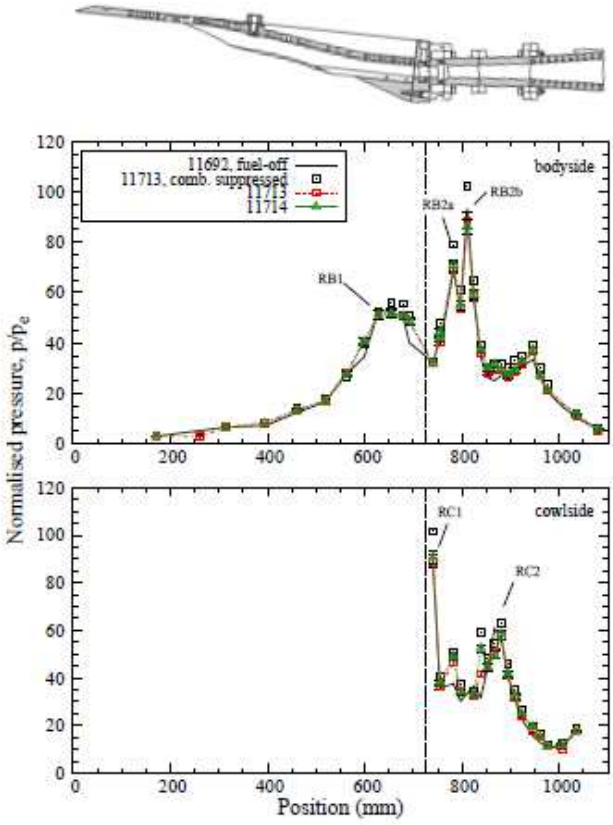

Fig. 12 Methane-fueled experiments

C. Methane-fueled experiments

When methane is injected, there is no observable combustion-induced pressure rise; only pressure rise due to mass addition is evident. This can be seen by comparison of shots 11713, 11714, and 11715, the last of which, has had combustion suppressed through the use of a nitrogen test gas. Due to the methodology used to design the cavity flameholder, methane was not expected to auto-ignite. Methane fueled experiments were still conducted, however, to verify the need for forced ignition for this fuel choice.

D. Comparison of fuels

To aid with comparison, tests with gaseous hydrogen were also performed for the engine with the cavity. The pressure distributions for hydrogen (shot 11727), ethylene (shot 11700), and methane (shot 11714) are shown in Fig. 13. The pressure distributions upstream of the injection point ($x = 725$ mm) are near identical, as expected. The pressure distributions vary greatly following the injection of fuel at the combustor entrance. A fuel-off shot is used for comparison (shot 11692), as

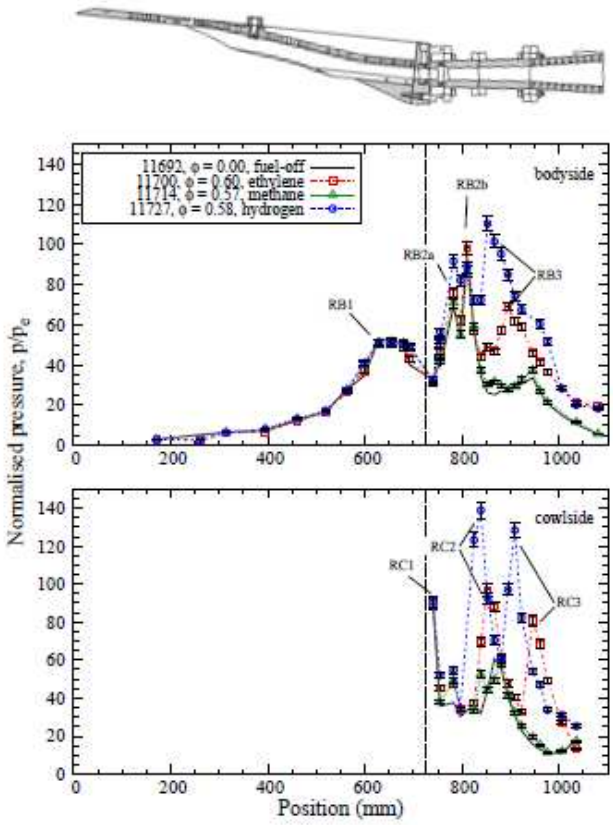

Fig. 13 Comparison of fuels tested

the three fuels only exhibit small differences between their associated suppressed-combustion shots.

As discussed in Section VI B, ethylene ignites and burns from $x = 850$ mm on both the body and cowlside of the engine, with the flowfield on the cowlside of the engine being heavily shock-dominated. The pressure distribution from the hydrogen-fueled experiment shown in Fig. 13 shows hydrogen igniting at the cavity flameholder ($x = 750$ mm). The ignition of hydrogen also occurs approximately 25 mm earlier than ethylene, which occur at 800 mm and 825 mm, respectively. The flowfield downstream of the cavity appears to have been altered by the combustion of hydrogen at the cavity. The recompression shock of the cavity (RB2b) appears to arrest the combustion of hydrogen immediately downstream of the cavity; the normalized pressure drops to combustion-suppressed levels.

Both hydrogen and ethylene achieve the same pressure rise on the body side of the engine from 1000 mm to the end of the flowpath. This could suggest that although ethylene ignites further downstream then hydrogen, it may burn just as completely as hydrogen. On the cowlside of the

engine, ethylene exhibits a higher pressure for the most of the nozzle, however, the pressure drops to suppressed combustion levels by the nozzle exit.

VII. Conclusions

The main objective of this study was to demonstrate the combustion of gaseous hydrocarbon fuels in a "real" engine operating at a high Mach number flight condition. Previous testing with this engine extensively examined the performance of hydrogen fuel. In order to ignite and burn hydrocarbons the combustor was modified to include a cavity flameholder. This series of testing demonstrates that a cavity flameholder promotes the ignition of gaseous ethylene fuel at a flight Mach number of 7.3, with fuel-air equivalence ratios ranging from 0.60-0.70. The results of the current work suggest that the passive entrainment of fuel and air into the cavity sufficiently increases the effective residence time of engine, such that the combustion of ethylene may occur.

Acknowledgments

This work was supported by the AOARD under Grant No. FA2386-13-1-4060, with David Hopper as contract manager, and Chiping Li (AFOSR) as program manager. Zachary Denman is supported by the Australian Government through the Australian Postgraduate Award (APA). The authors would also like to acknowledge the help of UQ technicians, Keith Hitchcock and Barry Allsop, the T4 Reflected Shock Tunnel operators (Kevin Basore, Will Landsberg, Tamara Sopek, Tristan Vanyai). This research was undertaken with the assistance of resources provided at the NCI National Facility systems at the Australian National University through the National Computational Merit Allocation Scheme supported by the Australian Government.

References

[1] Billig, F. S., "Research on Supersonic Combustion," *Journal of Propulsion and Power*, Vol. 9, No. 4, 1993, pp. 499-514. doi: 10.2514/3.23652

[2] Mehta, U. B., "Strategy for Developing Air-Breathing Aerospace Planes," *Journal of Aircraft*, Vol. 33, No. 2, 1996, pp. 377-385. doi: 10.2514/3.46948

[3] Jazra, T., Preller, D., Smart, M. K., "Design of an Airbreathing Second Stage for a Rocket-Scramjet-Rocket Launch Vehicle," *Journal of Propulsion and Power*, Vol. 50, No. 2, 2013, pp. 411-422. doi: 10.2514/1.A32381

[4] Curran, E. T., "Scramjet Engines: The First Forty Years," *Journal of Propulsion and Power*, Vol. 17, No. 6, 2001, pp.1138-1148. doi: 10.2514/2.5875

[5] Lewis, M. J., "Significance of Fuel Selection for Hypersonic Vehicle Range," *Journal of Propulsion and Power*, Vol. 17, No. 6, 2001, pp. 1214-1221. doi: 10.2514/2.5866

[6] Turns, S. R., "An Introduction to Combustion: Concepts and Applications," McGraw-Hill, 2nd ed., 2000.

[7] Powell, O. A., Edwards, J. T., Norris, R. B., Numbers, K. E., Pearce, J. A., "Development of Hydrocarbon-Fueled Scramjet Engines: The Hypersonic Technology (HyTech) Program," *Journal of Propulsion and Power*, Vol. 17, No. 6, 2001, pp. 1170-1176. doi:10.2514/2.5891

[8] Tishkoff, J. M., Drummond, J. P., Edwards, T., Nejad, A. S., "Future Directions of Supersonic Combustion Research: Air Force/NASA Workshop on Supersonic Combustion," *35th Aerospace Sciences Meeting and Exhibit*, 1997. doi: 10.2514/6.1997-1017

[9] Ben-Yakar, A., Hanson, R. K., "Cavity Flame-Holders for Ignition and Flame Stabilization in Scramjets: An Overview," *Journal of Propulsion and Power*, Vol. 17, No. 4, 2001, pp. 869-877. doi: 10.2514/2.5818

[10] Davis, D. L., Bowersox, R. D. W., "Stirred Reactor Analysis of Cavity Flame Holders for Scramjets," *33rd Joint Propulsion Conference and Exhibit*, 1997, pp. 1-14. doi: 10.2514/6.1997-3274

[11] Davis, D. L., Bowersox, R. D. W., "Computational Fluid Dynamics Analysis of Cavity Flame Holders for Scramjets," *33rd Joint Propulsion Conference and Exhibit*, 1997. pp. 1-14. doi: 10.2514/6.1997-3270

[12] Colket, M. B., Spadaccini, L. J., "Scramjet Fuels Autoignition Study," *Journal of Propulsion and Power*, Vol. 17, No. 2, 2001, pp. 315-323. doi: 10.2514/2.5744

[13] Gruber, M. R., Baurle, R. A., Mathur, T., Hsu, K.-Y., "Fundamental Studies of Cavity-Based Flameholder Concepts for Supersonic Combustion," *Journal of Propulsion and Power*, Vol. 17, No. 1, 2001, pp. 146-153. doi: 10.2514/2.5720

[14] Zhang, X., Rona, A., Edwards, J. A., "The Effect of Trailing Edge Geometry on Cavity Flow Oscillation Driven by a Supersonic Shear Layer," *Aeronautical Journal*, Vol. 102, No. 1011, pp. 129-136.

[15] Samimy, M., Petrie, H. L., Addy, A.L., "A Study of Compressible Turbulent Reattaching Free Shear Layers," *AIAA Journal*, Vol. 24, No.2, 1986, pp. 261-267. doi: 10.2514/6.1985-1646

[16] Voland, R. T., Auslender, A. H., Smart, M. K., Roudakov, A. S., Semenov, V. L., Kopchenov, V., "CIAM/NASA Mach 6.5 Scramjet Flight and Ground Test," *9th International Space Planes and Hy-*

personic Systems and Technologies Conference, 1999, pp. 1-9. doi: 10.2514/6.1999-4848

[17] Mathur, T., Gruber, M., Jackson, K., Donbar, J., Donaldson, W., Jackson, T., Billig, F., "Supersonic Combustion Experiments with a Cavity-Based Fuel Injector," *Journal of Propulsion and Power*, Vol. 17, No. 6, 2001, pp. 1305-1312. doi: 10.2514/2.5879

[18] Gruber, M. R., Donbar, J. M., Carter, C. D., Hsu, K.-Y., "Mixing and Combustion Studies Using Cavity-Based Flameholders in a Supersonic Flow," *Journal of Propulsion and Power*, Vol. 20, No. 5, 2004, pp. 769-778. doi: 10.2514/1.5360

[19] Gruber, M., Smith, S., and Mathur, T., "Experimental Characterization of Hydrocarbon-Fueled, Axisymmetric Scramjet Combustor Flowpaths," *17th AIAA International Space Planes and Hypersonic Systems and Technologies Conference, San Francisco, California*, 2011, pp. 1-24. doi: 10.2514/6.2011-2311

[20] Gollan, R. J., Jacobs, P. A., "About the formulation, verification and validation of hypersonic flow solver Eilmer," *International Journal for Numerical Methods in Fluids*, Vol. 73, No. 1, 2013, pp. 19-57. doi: 10.1002/fld.3790

[21] Turner, J. C., Smart, M. K., "Application of Inlet Injection to a 3-D Scramjet at Mach 8," *AIAA Journal*, Vol. 48, No. 4, 2010, pp. 829-838. doi: 10.2514/2.5774

[22] Stern, F., Wilson, R. V., Coleman, H. W., Paterson, E. G., "Comprehensive Approach to Verification and Validation of CFD Simulations - Part 1: Methodology and Procedures," *Journal of Fluids Engineering*, Vol. 123, No. 4, 2001, pp. 792-802. doi: 10.1115/1.1412235

[23] M. K. Smart, "Design of Three-Dimensional Hypersonic Inlets with Rectangular-to-Elliptical Shape Transition," *Journal of Propulsion and Power*, Vol. 15, No. 4, 1991, pp. 408-416. doi: 10.2514/2.5459

[24] Chan, W. Y. K., Razzaqi, S. A., Smart, M. K., Wise, D. J., "Freejet testing of the 75%-scale HIFiRE 7 rest scramjet engine," *19th AIAA International Space Planes and Hypersonics Systems and Technologies Conference, Atlanta, Georgia*, 2014, pp. 1-20. doi: 10.2514/6.2014-2931

[25] Stalker, R. J., Paull, A., Mee, D. J., Morgan, R. G., Jacobs, P. A., "Scramjets and shock tunnels - The Queensland experience," Progress in Aerospace Sciences, Vol. 41. 2005, pp. 471-513. doi:10.1016/j.paerosci.2005.08.002

[26] Jacobs, P. A., Gollan, R. J., Potter, D. F., Zander, F., Gildfind, D. E., Blyton, P., Chan, W. Y. K., Doherty, L., "Estimation of high-enthalpy flow conditions for simple shock and expansion processes using the ESTCj program and library," *Department of Mechanical Engineering Report 2011/2*, University of Queensland, 2011

[27] Jacobs, P. A., Rogers, R. C., Weidner, E. H., Bittner, R. D., "Flow Establishment in a Generic Scramjet Combustion," *Journal of Propulsion and Power*, Vol. 8, No. 4, 2011, pp. 890-899. doi: 10.2514/3.23566